DOT/FAA/TC-24/21

Federal Aviation Administration
William J. Hughes Technical Center
Aviation Research Division
Atlantic City International Airport
New Jersey 08405

Measuring the Fire Growth Potential of Combustible Solids Using a Cone Calorimeter

August 2024

Internal report

U.S. Department of Transportation
Federal Aviation Administration

NOTICE

This document is disseminated under the sponsorship of the U.S. Department of Transportation in the interest of information exchange. The U.S. Government assumes no liability for the contents or use thereof. The U.S. Government does not endorse products or manufacturers. Trade or manufacturers' names appear herein solely because they are considered essential to the objective of this report. The findings and conclusions in this report are those of the author(s) and do not necessarily represent the views of the funding agency. This document does not constitute FAA policy. Consult the FAA sponsoring organization listed on the Technical Documentation page as to its use.

This report is available at the Federal Aviation Administration William J. Hughes Technical Center's Full-Text Technical Reports page: actlibrary.tc.faa.gov in Adobe Acrobat portable document format (PDF).

Form DOT F 1700.7 (8-72) Reproduction of completed page authorized

1. Report No.	2. Government Accession No.	3. Recipient's Catalog No.
DOT/FAA/TC-24/21		

4. Title and Subtitle	5. Report Date
Measuring The Fire Growth Potential of Combustible Solids Using a Cone Calorimeter	May 2024
	6. Performing Organization Code ANG-E21

7. Author(s)	8. Performing Organization Report No.
Richard E. Lyon	

9. Performing Organization Name and Address	10. Work Unit No. (TRAIS)
Fire Safety Branch, ANG E-21 William J. Hughes Technical Center Atlantic City International Airport, NJ 08405	11. Contract or Grant No.

12. Sponsoring Agency Name and Address	13. Type of Report and Period Covered
Aircraft Certification Service/AVS FAA Northwest Mountain Regional Office 2200 S 216th St Des Moines WA 98198-6547 USA	14. Sponsoring Agency Code

15. Supplementary Notes

16. Abstract

The fire growth rate of interior linings, furnishings, and construction materials is measured in full-scale fire tests such as the ASTM E84 Steiner Tunnel, the ISO 9705 room fire, and a passenger aircraft cabin as the flame spread rate, time-to-flashover, or time to incapacitation, respectively. The results are used to indicate the level of passive fire protection afforded by the combustible material or product in the test. These large-scale tests require many square meters of product, are very expensive to conduct, and can exhibit poor repeatability- making them unsuitable for product development, quality control, or product surveillance. For this reason, smaller (≈ 0.01 m^2) samples are tested in bench-scale fire calorimeters under controlled conditions, and these one-dimensional burning histories are correlated with the results of the two- and three-dimensional burning histories in full-scale fire tests by a variety of empirical and semi-empirical fire propagation indices, as well as analytic and computer models that are particular to the full-scale fire test.

A more general approach described here equates the coupled fire growth processes of surface flame spread and in-depth burning to the generation of combustion heat in response to the radiant energy from a fire calorimeter that is above the critical value for ignition and burning. This measurement in a cone calorimeter under standard conditions (ASTM E1354) is used to compute the fire growth potential of the combustible solid, λ (m^2/MJ), which is realized as a hazard when the heat of combustion, H_c (MJ/m^2), is sufficient to grow the fire. Consequently, the dimensionless fire hazard of a material or product is obtained directly from a single cone calorimeter measurement as $\Pi = \lambda H_c$. The physical basis for λ and Π as well as their method of evaluation in a cone calorimeter are described. Experimental data show that the development of full-scale compartment fires and free standing product fires correlates with Π as the sole explanatory variable. .

17. Key Words	18. Distribution Statement
Fire Testing – Fire Growth Rate Fire Testing – Cone Calorimeter	This document is available to the U.S. public through the National Technical Information Service (NTIS), Springfield, Virginia 22161. This document is also available from the Federal Aviation Administration William J. Hughes Technical Center at actlibrary.tc.faa.gov.

19. Security Classif. (of this report)	20. Security Classif. (of this page)	21. No. of Pages	22. Price
Unclassified	Unclassified	43	

Acknowledgements

The author would like to thank Tina Emami for conducting the FAR fire tests and Richard Walters, Timothy Salter and Sean Crowley for conducting the cone calorimeter tests.

Contents

Figures

Tables

Acronyms

Acronym	Definition
ANN	Artificial neural networks
ASTM	American Society for Testing and Materials
BFR	Brominated flame retardant
CFD	Computational fluid dynamics
EHF	External heat (energy) flux
FAA	Federal Aviation Administration
FAR	Federal Airworthiness Regulation
FGC	Fire growth capacity
FIGRA	Fire Growth Rate
FPI	Fire Propagation Index
FTP	Flux time product
HRR	Heat release rate
LOI	Limiting oxygen index
ML	Machine learning
NFR	No flame retardant
NIST	National Institute of Standards and Technology
PFR	Phosphorus flame retardant
PHRR	Peak (maximum) heat release rate
SBI	Single burning item
THR	Total heat released by burning per unit surface area
TTI	Time to piloted ignition in a cone calorimeter

Executive summary

The growth rate of fires involving combustible materials in aircraft cabins was measured in full-scale tests at the FAA Technical Center during the 1980s, and the results of these full-scale tests were the basis for the bench-scale flammability requirements codified in Title 14 of the Code of Federal Regulation, Part 25 (14 CFR 25). These regulatory bench scale fire-tests are supposed to indicate the level of passive fire protection afforded by a combustible cabin material in a post-crash or in-flight fire, and they are used by aircraft manufacturers and suppliers for product development, quality control, regulatory compliance, and product surveillance. However, unlike full-scale cabin fires in which surface flame spread and in-depth burning are coupled processes that determine the rate of fire growth, the various 14 CFR 25 bench-scale fire tests measure these processes separately, so individually they have limited correlation with passenger escape time.

To better predict the passenger escape time in a post-crash cabin fire and the time available for an emergency landing in the event of an in-flight fire, a fire growth potential $\lambda(m^2/J)$ is derived that is the surface flame-spread rate of a material (m^2/s) per unit radiant power of a fire or heater (W). The potential for fire growth can be measured in one or more standard (ASTM E1354) fire calorimetry tests, but is only realized as a hazard if the heat of combustion per unit area of burning surface, H_c (J/m^2) is sufficient to grow the fire. The predictor of full-scale fire performance is therefore the *product* fire hazard, $\Pi = \lambda H_c$, which is a dimensionless quantity that depends on the amount (thickness, b) of the material. A *material* fire hazard is independent of the amount (volume) of sample, and a good predictor of material fire performance is, $\pi = \Pi/b$. This report describes the physical basis for λ, Π, and π as well as their method of evaluation in one or more ASTM E1354 fire calorimeter tests. The utility of π for ranking and classifying material flammability, and the efficacy of Π as a criterion for the onset of full-scale fire growth are described.

1 Introduction

When considering new materials for occupied spaces, fire performance is one of several factors that need to be considered. There are various approaches for assessing the passive fire protection capability of materials and their structural elements. The prescribed method is to conduct experiments in accordance with fire standards and regulations (Compartment Interiors, 2004; ISO-5660-1, 2002; ASTM E906, 2017). Numerical simulations, e.g., computational fluid dynamics (CFD), coupled to pyrolysis models (McGrattan, McDermott, Weinschenk, & Forney, 2013) are another approach that allows researchers to carry out simulations using physical and chemical properties of materials that must be estimated or determined experimentally (Stoliarov & Ding, 2023). More recently, the fire performance of combustible materials has been simulated using artificial intelligence, machine learning (ML), and artificial neural networks (ANN) (Nguyen, Nguyen, Le, & Zhang, 2021). However, the descriptors used to train the model may be non-physical or nonsensical.

The most common method to estimate the fire growth potential of materials is to measure the heat-release rate history in fire calorimeters under controlled conditions (ASTM E906, 2017; ISO-5660-1, 2002). The cost advantage of using small/bench scale 0.01 m^2 specimens to predict the outcome of large/full-scale fire tests requiring many square meters of material (ISO 9705-1, 2016; ASTM 2257, 2022) is significant, so various bench-scale fire test parameters have been proposed to rank or classify the flammability and ignitability of combustible materials (Numjiri & Furukawa, 1998; Agarwal, Wang, & Dorofeev, 2021; Tewarson, Kahn, Wu, & Bill, Jr., 2001) as well as their performance in full-scale fire tests (ASTM E1354, 2023). These empirical and semi-empirical formulas are meaningful only for materials of the same or similar composition tested under identical conditions.

A fire propagation index, FPI = ($\dot{Q}_{max}/t_{ign}$) (Tewarson, Kahn, Wu, & Bill, Jr., 2001) and its inverse ($\dot{Q}_{max}/t_{ign}$)$^{-1}$ (Hirschler, 1992; Hirschler, 1995) have been proposed as predictors of the time to reach untenable conditions (flashover) in full-scale room fire tests of furnishings and wall lining materials, where $\dot{Q}_{max}$(W/m^2) is the maximum heat release rate per unit area and t_{ign} is the time to piloted ignition measured in a cone calorimeter according to ISO 5660 (2002) or ASTM E1354 (2023). Recently, Vahabi et.al. (2019; 2023) added the heat of combustion H_c to the FPI as suggested earlier by Petrella (1994), and obtained a fire retardancy parameter, FR = $\dot{Q}_{max}H_c/t_{ign}$ that improved the correlation of FPI with fire test data.

Tewarson et.al. (2001) used FPI = 750 $\dot{Q}^{1/3}/\dot{q}_{net}t_{ign}^2$ measured in a bench scale fire propagation apparatus ASTM E2058 (2019) at net heat flux $\dot{q}_{net}$ to correlate upward fire growth in a full-

scale (2.4 m x 0.6 m x 2) parallel panel test that is used to qualify clean room materials for fire safety (ANSI/FM Approvals 4910-2004, 2004).

Numajiri and Furukawa (1998) used an empirical function to fit the heat-release rate history in a cone calorimeter and use the fitting parameters to compute a burning index.

Ostman et.al. (1994; 1995) used an empirical equation to correlate cone calorimeter data for wood, construction and wall lining materials measured at an external heat flux $\dot{q}_{ext}$ = 50 kW/m^2 with the time to reach 1 MW heat release rate (flashover) in a full-scale room fire test (ISO 9705-1, 2016; ASTM 2257, 2022; NFPA 286) that is used to classify the fire safety of these products.

Shields et.al. (1994) recognized the importance of ignitability on fire growth and used a flux time product, FTP = $t_{ign}\left(\dot{q}_{ext} - \dot{q}_{ign}\right)^N$, to evaluate the critical heat flux for ignition $\dot{q}_{ign}$ of wood by measuring t_{ign} as a function of $\dot{q}_{ext}$ with N an empirical parameter related to sample thickness. The FTP was shown to be independent of sample orientation with respect to gravity and the mode of ignition (spark or flame).

To bridge the length scale between a bench-scale fire calorimeter (0.01m^2) and a full-scale room fire test (32m^2), a quarter-scale fire test using an 8 m^2 sample was developed called the single burning item (SBI) (CEN-EN 13823:2020+A1:2022). The fire growth rate (FIGRA) of a material in the SBI test was defined as the maximum value of the heat release rate (HRR) of the SBI ignited by a gas burner in the corner of a standard fixture divided by the time to reach the maximum. Despite many caveats to the measurement, the FIGRA value is used to classify the fire safety of building products as A1, A2, B, C, and D in Europe. However, the SBI test, like the room fire test, is expensive, so a computer model was developed to calculate the HRR in the SBI and ISO 9705 test from a single cone calorimeter heat-release rate history (Van Hees, Hertzberg, & Steen, 2002).

The purpose of bench-, product-, quarter-, and full-scale fire tests of combustible solids, as well as numerical modeling of fire growth (McGrattan, McDermott, Weinschenk, & Forney, 2013; Stoliarov & Ding, 2023; Van Hees, Hertzberg, & Steen, 2002; Stoliarov, Leventon, & Lyon, 2013), is to measure or predict the level of passive fire protection afforded by a specific composition of combustible matter in a particular fire environment. This paper attempts to achieve that goal analytically using ignition and burning theory to account for these coupled processes in fire growth and to propose a method of evaluating the fire growth potential of combustible solids using a cone calorimeter under standard conditions.

2 Technical approach

The fire growth of combustible solids is a two-dimensional process of anaerobic in-depth fuel generation and surface flame spread at a solid-air interface, where the gaseous fuel mixes with oxygen and reacts in a flame to generate heat and products of complete and incomplete combustion. The fuel generation (burning) rate is coupled to the flame spread rate by heat transfer from the flame or fire to the solid surface, which depends on the angle of inclination with respect to gravity. The classic formalisms of liquid and solid burning describe the steady state heat release rate per unit area $\dot{Q}_{ss}$(W/m^2) as it relates to the steady burning rate per unit area $\dot{m}_{ss}$ (kg/m^2-s) and the effective heat of combustion of the fuel gases with oxygen in a diffusion flame h_c (J/kg) (Drysdale, 2011; Quintiere, 2006),

$$\dot{Q}_{ss} = \dot{m}_{ss} h_c \qquad 1$$

By convention, the fluxes of combustion heat ($\dot{Q}$) and volatile fuel mass ($\dot{m}$) are positive, as is the specific heat of combustion (h_c). A diffusion flame attaches to the surface after the fuel gases ignite at the solid surface. The mass flux is proportional to the net surface heat flux ($\dot{q}_{net}$) and inversely proportional to the energy required to thermally decompose the solid to gaseous fuel and vaporize the products, h_g (J/kg). For steady burning,

$$\dot{m}_{ss} = \frac{\dot{q}_{net}}{h_g} \qquad 2$$

Substituting Equation 2 into Equation 1 for a solid of surface area S, density ρ, and pyrolysis depth δ, the steady heat release rate is,

$$\dot{Q}_{ss} = \frac{h_c}{h_g}\dot{q}_{net} = \left(\frac{\chi}{\alpha}\right)\left(\frac{\rho b h_c}{\rho b h_g}\right)\dot{q}_{net} = \left(\frac{H_c}{H_g}\right)\dot{q}_{net} \qquad 3$$

In Equation 3, b is the sample thickness, χ is the efficiency of combustion in a diffusion flame and α is the efficiency of heat transfer at the heated surface, $x = 0$. The last term assumes $\chi/\alpha = 1$. The slope of a plot of $\dot{Q}_{ss}$ *versus* $\dot{q}_{net}$ is the called the combustibility ratio (Rasbash, 1976) or heat release parameter (Tewarson, 1980). It is the ratio of the heat released by combustion of the fuel gases in air to the energy consumed to generate the fuel gases in the solid at the burning temperature on a mass (h_c/h_g) or areal (H_c/H_g) basis in the pyrolysis volume, $V_p = \delta S$. Once burning has commenced, the surface of the solid $x = 0$ is at the burning temperature T_{burn} and the pyrolysis layer extends into the solid to a depth $x = \delta$ that is at the ignition temperature, T_{ign}. Both T_{burn} and T_{ign} are determined by the chemical kinetics of thermal decomposition of the solid (Lyon, 2000; Lyon & Crowley, 2021; ASTM D7309-23, 2023).

Equation 3 is predicated on the existence of a steady heat release rate, $\dot{Q}_{ss}$. A steady heat release rate in a cone calorimeter can be approximated for $\dot{Q}(t)$ as a time average of the heat release rate history (Whiteley, Elliot, & Staggs, 1996) or a moment average of the heat release history (Lyon, Crowley, & Walters, 2008) to obtain $\dot{Q}_{ss}$ as a test average value, $\dot{Q}_{avg}$, or a moment average of the heat release rate in the vicinity of the maximum/peak heat release rate, $\dot{Q}_{max}$,

$$\dot{Q}_{ss} = \frac{5}{2\sqrt{3}}\dot{Q}_{avg} = \frac{1}{\sqrt{3}}\dot{Q}_{max} \qquad 4$$

The thermal theory of ignition assumes the ignition temperature T_{ign} is a property of the material, consistent with the kinetic basis for T_{ign} as the temperature at the onset of thermal decomposition of the solid (Lyon, Safronava, Crowley, & Walters, 2021; Lyon, Safronava, & Crowley, 2018). Consequently, the time required for the surface of a solid of thickness b, specific heat c_P, and thermal conductivity κ, initially at temperature T_0 to reach T_{ign} when exposed to a constant net heat flux $\dot{q}_{net}$ at $t = 0$ in a cone calorimeter increases with the thermal stability of the solid and is obtained from unsteady heat conduction as the time to ignition, t_{ign} (Drysdale, 2011; Quintiere, 2006),

$$t_{ign} = \begin{cases} \rho c_P b\, \Delta T_{ign}/\dot{q}_{net} & (thermally\ thin, b < \delta) \\ \rho c_P \kappa \left(\Delta T_{ign}/\dot{q}_{net}\right)^2 & (thermally\ thick, b \geq \delta) \end{cases} \qquad 5$$

The depth of the pyrolysis layer at ignition for $\dot{q}_{net} = \kappa \Delta T_{ign}/\Delta x$ (Lyon, 2000) is

$$\Delta x = \delta = \frac{\kappa\left(T_{ign} - T_0\right)}{\dot{q}_{net}} = \frac{\kappa\, \Delta T_{ign}}{\dot{q}_{net}} \qquad 6$$

The thermal energy that has entered the surface of a combustible solid at the time of ignition t_{ign} in a cone calorimeter when a constant net influx of heat $\dot{q}_{net}$ is instantaneously applied at time $t = 0$ is the energy barrier to ignition (ignition energy) (Lyon & Crowley, 2021),

$$E_{ign} \equiv \int_0^{t_{ign}} \dot{E}\, dt = \int_0^{t_{ign}} \dot{q}_{net}\, dt = \dot{q}_{net} t_{ign} \qquad 7$$

Equations 1-7 describe the ignitability ($1/E_{ign}$) and combustibility ($H_c/H_g = \dot{Q}_{ss}/\dot{q}_{net}$) in terms of the energy supplied to, and released from, a combustible solid in a fire or fire calorimeter. Ignition and in-depth burning are the coupled processes driving flame spread and heat release rate in a fire, so it is the product of ignitability and combustibility that is the potential for fire growth in units of m^2/MJ,

$$\text{Fire Growth Potential, } \lambda \equiv \left(\frac{H_c}{H_g}\right)\left(\frac{1}{E_{ign}}\right) = \frac{H_c/H_g}{\dot{q}_{net} t_{ign}} = \frac{\dot{Q}_{ss}}{\dot{q}_{net}^2 t_{ign}} \qquad 8$$

The denominators of the last two terms of Equation 8 are the flux-time product at ignition, FTP = $t_{ign}\dot{q}_{net}^{N}$, for thermally thin (N=1) and thermally thick (N=2) samples at a constant net heat flux (Tewarson, 1994). The FTP is independent of sample orientation with respect to gravity (vertical or horizontal) and the mode of ignition (spark or flame) (Shields, Silcock, & Murray, 1994). Substituting Equation 5 for the time to ignition into Equation 7 gives explicit form to the ignition energy for a thermally thick combustible solid, $b \geq \delta$,

$$E_{ign} = \frac{\rho c_P \kappa \Delta T_{ign}^2}{\dot{q}_{net}} = \frac{TRP^2}{\dot{q}_{net}} \qquad 9$$

In Equation 9, TRP is called the thermal response parameter (Tewarson, 1994). Substituting Equation 9 into Equation 8 gives the fire growth potential of a thermally thick combustible solid that would be capable of steady burning,

$$\lambda = \frac{H_c/H_g}{E_{ign}} = \left[\frac{h_c/h_g}{\rho c_P \kappa \Delta T_{ign}^2}\right] \dot{q}_{net} = K\dot{q}_{net} = K\left(\dot{q}_{ext} - \dot{q}_{ign}\right) \qquad 10$$

Equation 10 is a constitutive relationship for the fire response λ to a thermal stress $\dot{q}_{net}$ that is the difference between an external energy flux $\dot{q}_{ext}$ and the critical energy flux for piloted ignition, $\dot{q}_{ign}$, for a combustible solid having fire compliance K. The fire growth potential is independent of sample thickness because the chemical reactions that generate volatile fuel are confined to a thin surface layer of depth $\delta << b$ for $\dot{q}_{net}$ > 50 kW/m^2 (typically), and the rate of these anaerobic reactions depends only on temperature. The fire response of a thermally thin solid is obtained from Equation 5, Equation 7, and Equation 8:

$$\lambda' = \frac{1}{b}\left[\frac{h_c/h_g}{\rho c_P \Delta T_{ign}}\right] = \frac{K'}{b} \qquad \text{(thermally thin)} \qquad 11$$

The fire response of a thin sample, $b < \delta$, is independent of thermal stress $\dot{q}_{net}$ and inversely proportional to the sample thickness b. The bracketed terms K and K', in Equation 10 and Equation 11, respectively, are intensive fire compliances because they are independent of the amount of combustible material, the sample orientation with respect to gravity, and the mode of ignition.

The fire growth potential of a combustible solid λ is only realized as a fire hazard if the heat of combustion per unit surface area H_c (MJ/m^2) is sufficient to sustain the fire, so the dimensionless fire hazard of a product is,

$$\text{Product Fire Hazard } = \Pi \equiv \lambda H_c \qquad 12$$

Unlike the fire growth potential λ, the fire hazard Π is not an intensive property because the amount of heat released by combustion depends on the mass or thickness of the material, i.e., the

fire load, H_c. Normalizing Equation 12 for thickness results in an average fire hazard of the material(s) comprising the product that is an intensive property computed from the volumetric heat of combustion, $H_{c,v}$ (MJ/m^3),

$$\pi = \lambda H_{c,v} = \Pi/b \qquad 13$$

3 Reduction to practice

At incipient ignition, the net flux of thermal energy $\dot{q}_{net}$ entering a surface exposed to a constant radiant/convective energy flux from an external heater or fire will be a fraction α of the incident energy flux, $\dot{q}_{ext}$, due to losses from the surface by re-radiation and convection, $\dot{q}_{loss}$,

$$\dot{q}_{net}(ignition) = -\kappa\left(\frac{dT}{dx}\right) = \kappa\frac{\Delta T_{ign}}{\delta} = \dot{q}_{ext} - \dot{q}_{loss} \equiv \alpha\dot{q}_{ext} \qquad 14$$

In Equation 14, α is the coupling efficiency of radiant energy with the combustible solid. According to Equation 7 and Equation 14 , the thermal energy absorbed by a solid in a cone calorimeter experiment at the time of ignition t_{ign} is related to the apparent value of the ignition energy, $E_{ign,0}$, at constant $\dot{q}_{ext}$,

$$E_{ign} = \alpha E_{ign,0} = \alpha\dot{q}_{ext}t_{ign} \qquad 15$$

At the onset of burning the flame adds an additional heat flux to the surface that increases its temperature from T_{ign} to T_{burn} (Lyon, Safronava, Crowley, & Walters, 2021). The surface temperature rise at the onset of steady burning therefore increases to, $\Delta T_{ss} = (T_{burn} - T_0) = (T_{burn} - T_{ign}) + (T_{ign}-T_0) = \Delta T_{burn} + \Delta T_{ign}$. If the heat flux from the flame provides all the energy required to thermally decompose the solid in the pyrolysis layer and gasify the products during steady burning, $\kappa\Delta T_{burn}/\delta = \dot{m}_{ss}h_g$ (Lyon, 2000),

$$\dot{q}_{net}(burning) = \left\{\kappa\frac{\Delta T_{burn}}{\delta} - \dot{m}_{ss}\,h_g\right\} + \kappa\frac{\Delta T_{ign}}{\delta} \approx \kappa\frac{\Delta T_{ign}}{\delta} = \alpha\dot{q}_{ext} \qquad 16$$

Figure 1 is an idealized heat release rate ($\dot{Q}$) history for ignition and burning under steady (Figure 1A) and unsteady (Figure 1B) conditions for an incident energy flux $\dot{q}_{ext}$ imposed at time $t = 0$ (Lyon & Crowley, 2021). The time-integrated histories of $\dot{Q}$ and the radiant energy flux, $\dot{E}_0 = \dot{q}_{ext}$ of Figures 1A and 1B are plotted as Q versus the nominal incident thermal energy, $E_0 = \dot{q}_{ext}t$, for the steady and unsteady processes in Figure 1C and 1D, with $E_{ign,0} = \dot{q}_{ext}t_{ign}$ the nominal ignition energy at the time of ignition, t_{ign}, and $E_{b,0} = \dot{q}_{ext}t_b$, the nominal incident energy at the end of burning t_b when the flame extinguishes. Steady burning is analogous to a phase change at a constant temperature, for which the boundary conditions at the surface $x = 0$ and the rear face $x = b$ remain constant, which is rarely (if ever) the case for

burning solids in the cone calorimeter because of the transient temperature gradient, rear face thermal insulation, and re-radiation at the fire-exposed surface.

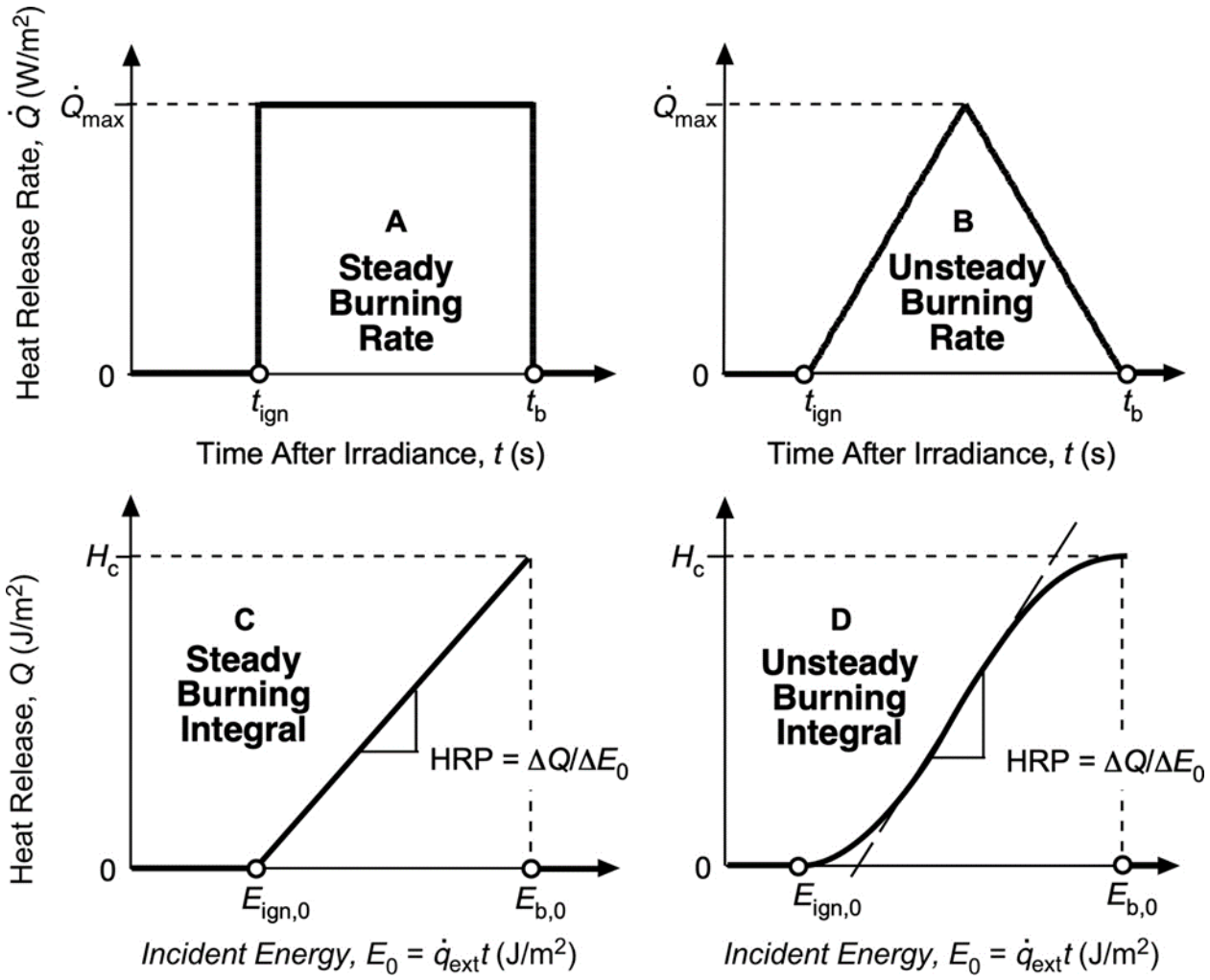

Figure 1. Idealized heat release histories for steady and unsteady burning

Substituting Equation 4 and Equation 14 into Equation 8 allows calculation of λ at constant irradiance ($\dot{q}_{ext}$) from the ignition energy E_{ign} and the slope of combustion heat versus the incident thermal energy, $\Delta Q/\Delta E_0$, or the test average heat release rate, $\dot{Q}_{avg}$, or the maximum/peak heat release rate in the test, $\dot{Q}_{max}$,

$$\lambda \equiv \frac{H_c/H_g}{E_{ign}} = \frac{1}{\alpha}\left(\frac{\Delta Q/\Delta E_0}{E_{ign,0}}\right) = \frac{1}{\alpha^2}\left(\frac{5}{2\sqrt{3}}\frac{\dot{Q}_{avg}}{\dot{q}_{ext}^2 t_{ign}}\right) = \frac{1}{\alpha^2}\left(\frac{1}{\sqrt{3}}\frac{\dot{Q}_{max}}{\dot{q}_{ext}^2 t_{ign}}\right) \quad 17$$

The coupling efficiency for a material in a cone calorimeter experiment α is probably in the range, ½ < α < 1 for charring and non-charring materials respectively (Lyon & Crowley, 2021; Stoliarov, Crowley , Lyon, & Linteris, 2009; Stoliarov, Crowley, Walters, & Lyon, 2010). Therefore, to a first approximation, α = ¾ and, $\sqrt{3}\alpha^2 \approx \sqrt{3}(3/4)^2 \approx 1$ in Equation 17, in which case the material fire response (λ) and product fire hazard (Π) can be expressed solely in terms of quantities that are measured in a standard cone calorimeter test, and whose acronyms and symbols are listed in Table 1.

$$\Lambda_{NRG} \equiv \frac{1}{\alpha}\left(\frac{H_c/H_g}{E_{ign}}\right) \approx \frac{4}{3}\frac{\Delta Q/\Delta E_0}{EHF*TTI} \quad 18$$

$$\lambda_{AVG} \equiv \frac{1}{\alpha^2\sqrt{3}}\left(\frac{5}{2}\frac{\dot{Q}_{avg}}{\dot{q}_{ext}^2\, t_{ign}}\right) \approx \frac{5}{2}\frac{HRR_{avg}/TTI}{EHF^2} \quad 19$$

$$\lambda_{MAX} \equiv \frac{1}{\alpha^2\sqrt{3}}\left(\frac{\dot{Q}_{max}}{\dot{q}_{ext}^2\, t_{ign}}\right) \approx \frac{PHRR/TTI}{EHF^2} \quad 20$$

The product fire hazards Π_j for j = energy (NRG) , AVG, and MAX of Equations 18-20 are,

$$\Pi_j = \lambda_j\, H_c = \left[\frac{H_c^2/H_g}{c_P \Delta T_{ign}}\right] \quad 21$$

Equation 21 is a physical interpretation of the dimensionless fire hazard of a product.

Table 1. Nomenclature of cone calorimeter test data

Quantity	**Acronym**	**Symbol**	**Units**
External Energy/Heat Flux	EHF	$\dot{q}_{ext}$	W/m^2
Maximum/Peak Heat Release Rate	PHRR	$\dot{Q}_{max}$	W/m^2
Test Average Heat Release Rate	HRR_{avg}	$\dot{Q}_{avg}$	W/m^2
Total Areal Heat Release/Fire Load	THR	H_c	J/m^2
Time-to-Piloted Ignition	TTI	t_{ign}	s

The assumptions leading to Equations 8-21 are examined experimentally for both charring and non-charring combustible materials. The fire growth potential (λ) as well as the product fire hazard (Π) and material fire hazard (π) are evaluated for some combustible materials and commercial products using cone calorimeter heat-release rate histories and test data from our laboratory and the published literature.

4 Experimental

4.1 Materials

The unmodified (natural) polymers in Table 2 contain no flame-retardant additives or fillers and minimal processing aids and were obtained in sheet form having nominal thickness 3.2, 6.4, 12.5, or 25 mm, from commercial suppliers. Polymer blends (PC/ABS) and flame-retardant polystyrene were provided by research partners.

Table 2. Polymers tested in this study

Polymer	**Symbol**	**Polymer**	**Symbol**
Acrylonitrile-butadiene-styrene polymer	ABS	Poly(hexamethylene adipamide)	PA66
High Density Polyethylene	HDPE	Poly(vinylidenefluoride)	PVDF
Polypropylene	PP	Poly(oxymethylene)	POM
PS with 20% Decabromodiphenyloxide	PS-BFR	Poly(phenylsulfone)	PPSU
High Impact Polystyrene	HIPS	Poly(phenylenesulfide)	PPS
Poly(methylmethacrylate)	PMMA	Poly(vinylchloride)	PVC
Polycarbonate of Bisphenol-A	PC	Polyetherimide	PEI
PC/ABS Blends	PC/ABS	Polyetheretherketone	PEEK
Poly(ethylene terephthalate)	PET	Fluorinated ethylene propylene	FEP

4.2 Methods

Tests were conducted in our laboratory at the Federal Aviation Administration (FAA) William J. Hughes Technical Center in triplicate on 10 cm x 10 cm square samples of various (typically 3.2 mm) thickness in a cone calorimeter from Fire Testing Technology, East Grinstead, UK, according to a standard method (ASTM E1354, 2023). A sample holder with edge frame and wire grid, insulated rear sample face, and a spark igniter were used for all tests. Cone calorimeter results from the literature were obtained under similar conditions. Gases used for calibration and testing were high purity grades from local suppliers.

5 Results

5.1 Metrology

Figure 2 is a composite of $\dot{Q}$ histories at four different heat flux levels $\dot{q}_{ext}$ for cast PMMA containing black pigment that is used as a cone calorimeter standard reference material. Each plot is an average of three experiments. Figure 3 is an energy diagram constructed from the time integrated $\dot{Q}$ and $\dot{E} = \dot{q}_{ext}$ histories in Figure 2 to obtain $E_{ign,0}$ and $\Delta Q/\Delta E_0$ for use in Equation 18 to calculate λ_{NRG}.

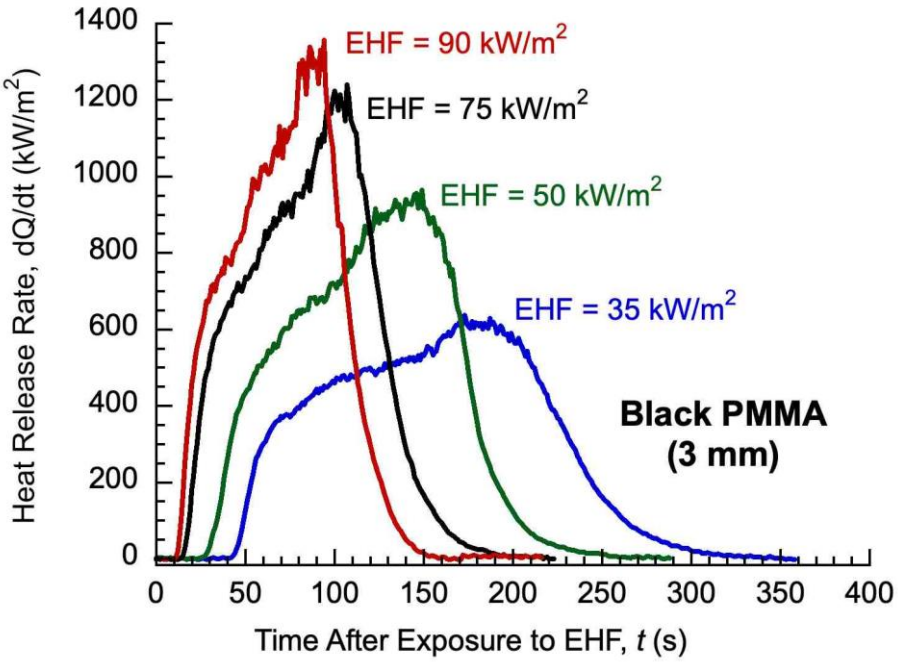

Figure 2. Heat release rate histories of black PMMA in cone calorimeter at $\dot{q}_{ext}$= EHF = 35, 50, 75 and 90 kW/m2.

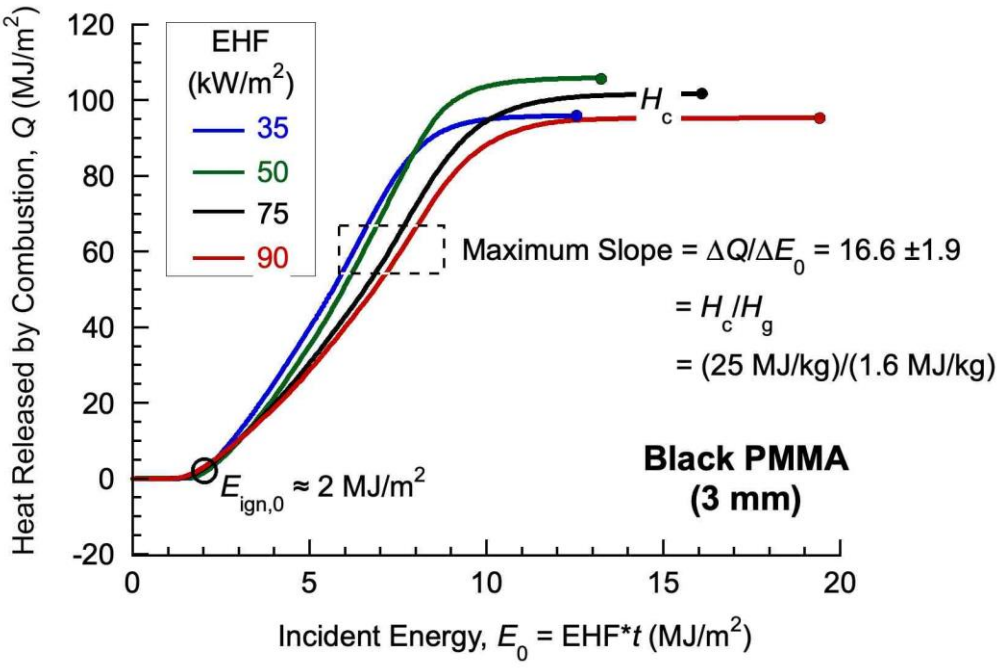

Figure 3. Cone calorimeter energy diagram of heat release versus incident energy showing nominal ignition energy ($E_{ign,0}$) and combustibility ($\Delta Q/\Delta E_0 = H_c/H_g$).

Energy diagrams like Figure 3 were constructed and evaluated for the 16 charring and non-charring polymers in Table 2 to obtain the nominal ignition energy, $E_{ign,0} = \dot{q}_{ext} t_{ign}$ = EHF t_{ign} and the nominal combustibility ratio, $H_c/H_g = \Delta Q/\Delta E_0$ as per Figure 2 for computing λ_{NRG} by Equation 18 .

Test average heat release rates, HRR_{avg} = (Total Heat Release)/(Total Burn Time) along with time to ignition t_{ign} = TTI at $\dot{q}_{ext}$ = EHF were obtained directly from cone calorimeter test reports and used to compute λ_{AVG} by Eqn. 19 for the 16 polymers in Table 2.

Peak heat release rate, $\dot{Q}_{max}$ = PHRR, as well as t_{ign} = TTI at $\dot{q}_{ext}$ = EHF were obtained directly from cone calorimeter test reports and used to compute λ_{PEAK} by Equation 20 for the 16 polymers of Table 2.

Figure 4 is a comparison of the three methods of computing λ from cone calorimeter measurements (i.e., Equations 18-20) for the 16 commercial polymers in Table 2. These polymers were tested in the cone calorimeter according to the standard method in triplicate at 3.2 mm thickness at the typical heat flux used in the literature, $\dot{q}_{ext}$ = 50 kW/m^2. The λ_j are ranked in descending order from top to bottom by λ_{MAX} (Equation 20). The three methods of λ calculation (Equations 18-20) show qualitative agreement for each polymer and consistent

ranking between polymers, with the three λ_j for each polymer typically within 20% of the mean value. Average coefficient of variation of λ_j for each individual polymer is less than 20%.

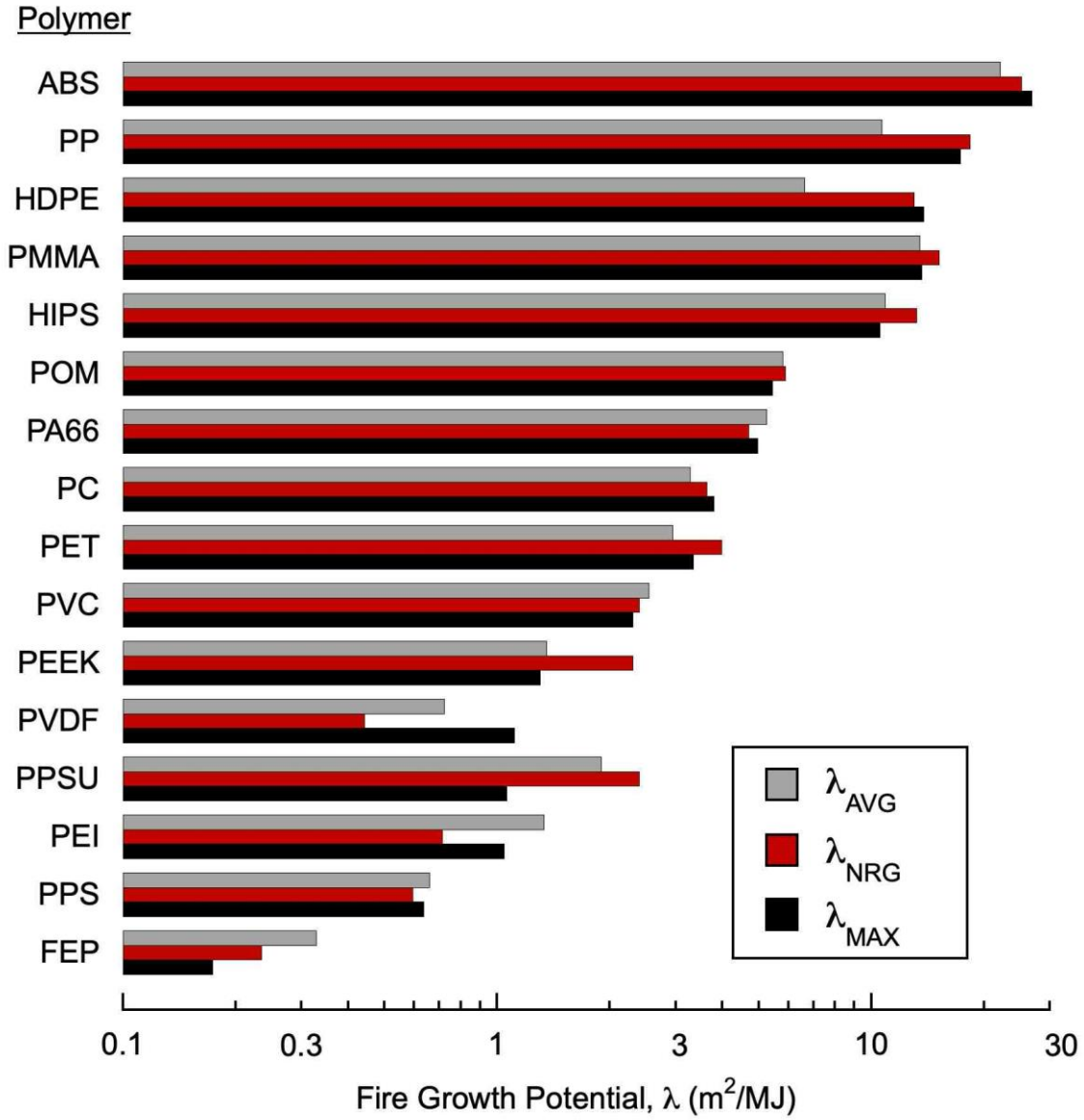

Figure 4. Fire growth potential λ of the 16 polymers in Table 2 tested at $\dot{q}_{ext}$ = 50 kW/m^2.

The 20% uncertainty in λ for an individual polymer using integrated (Equation 18) and moment-averaged (Equations 19 and 20) cone calorimeter data is typical of the uncertainty in λ from a propagation of error analysis using the reproducibility standard deviations for PHRR and TTI in ASTM E1354. For this reason, and to maximize the use of cone calorimeter data reported in the

published literature as λ_{MAX} at $\dot{q}_{ext}$ (50 kW/m^2, typically) Equation 20 is used to compute λ in the following plots and analyses unless otherwise specified.

5.2 Non-charring polymers

Figure 5 is a plot of ASTM E1354 (2023) cone calorimeter data for cast, black pigmented polymethylmethacrylate (PMMA) at 3, 6, and 25-mm nominal thickness at the external heat flux, $\dot{q}_{ext}$ = 50 kW/m^2. The left-hand ordinate of Figure 5 (λ) is the material fire response to incident thermal energy for PMMA. These samples are thermally thick at $\dot{q}_{ext}$ = 50 kW/m^2 because $b > \delta \approx \kappa \Delta T_{ign}/\dot{q}_{ext}$ = 1.2 mm for T_{ign} = 580K, κ = 0.2 W/m-K, so λ is independent of thickness in agreement with Equation 10. Conversely, the product fire hazard Π on the right-hand ordinate is proportional to sample thickness/fire load as per Equation 12.

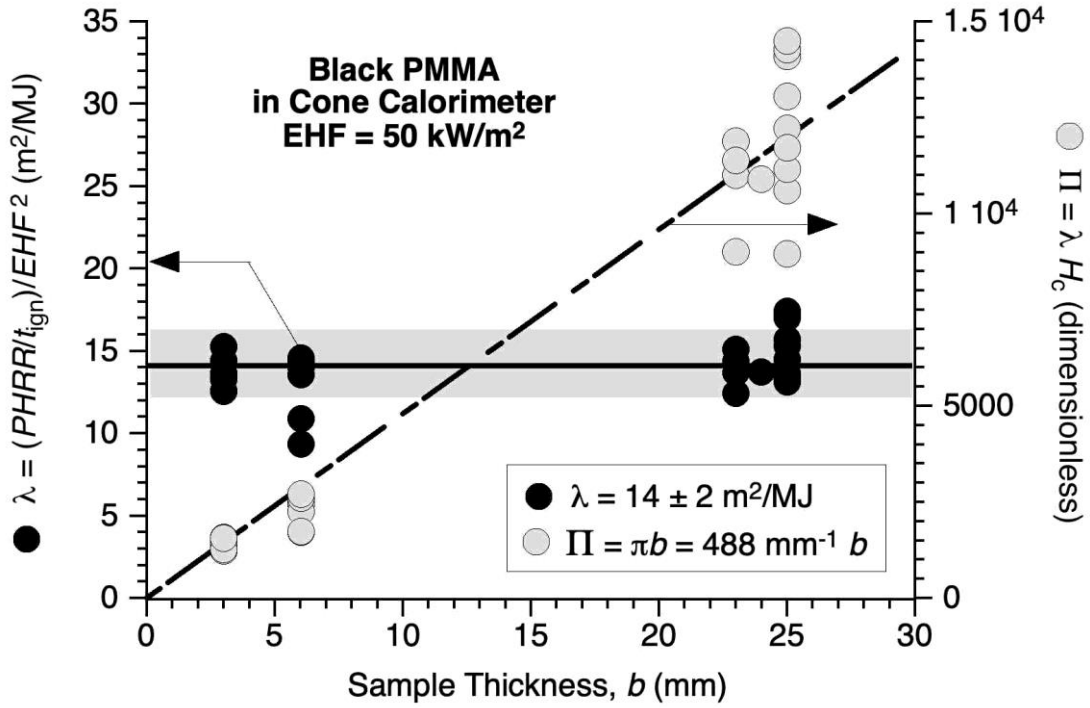

Figure 5. Fire growth potential λ and product fire hazard Π versus sample thickness b for black PMMA at $\dot{q}_{ext}$ = EHF = 50 kW/m^2.

Figure 6 is a plot of λ computed from published ASTM E1354 data (Stoliarov, Crowley , Lyon, & Linteris, 2009) obtained in our laboratory for clear extruded PMMA at nominal thickness, b = 3, 9, and 27 mm exposed to $\dot{q}_{ext}$ = 25, 50, and 75 kW/m^2. These samples are thermally thick under all conditions as per Equation 5 and as evidenced by the insensitivity of λ to b and the linear relationship between λ and $\dot{q}_{ext}$, as per the constitutive relation for fire growth, Equation 10. The zero-slope line of λ versus b and the linear fit to $\dot{q}_{ext}$ intersect at $\dot{q}_{ext}$ = 51 kW/m^2. Error bars are one standard deviation of the average value with respect to the independent variable on the opposite abscissa.

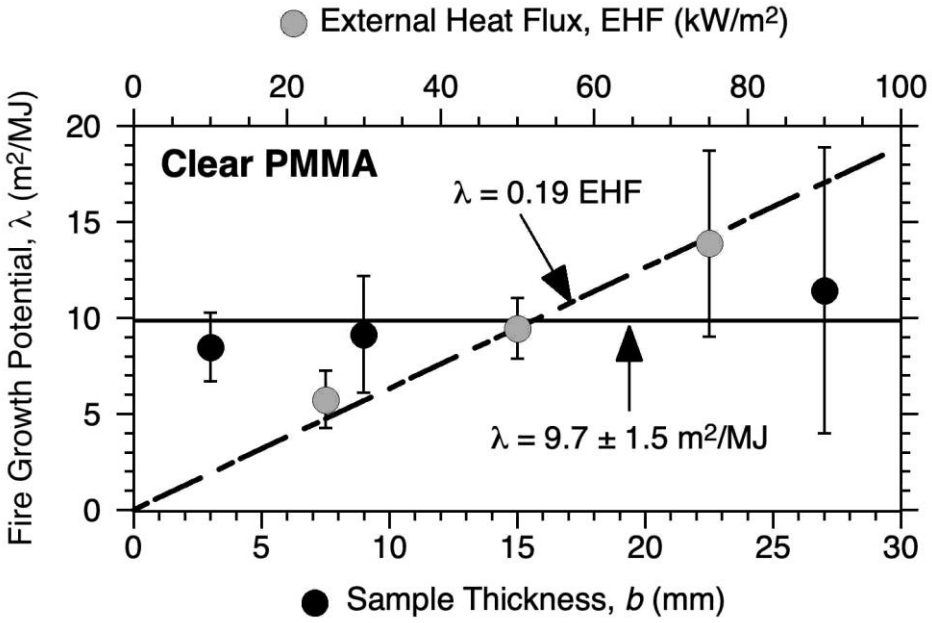

Figure 6. Fire growth potential λ versus $\dot{q}_{ext}$= EHF and sample thickness (b) for clear PMMA in ASTM E1354

Figure 7 is a plot of the nominal ignition energy, $E_{\text{ign},0} = \dot{q}_{ext} t_{ign}$ for clear PMMA at the same values of b and EHF shown in Figure 6. The horizontal line for λ versus b and the inverse relationship of $E_{\text{ign},0}$ to $\dot{q}_{ext}$ as per Equation 9, intersect at $\dot{q}_{ext}$ = 41 kWm^2. Error bars are one standard deviation of the indicated average with respect to the independent variable on the opposite abscissa.

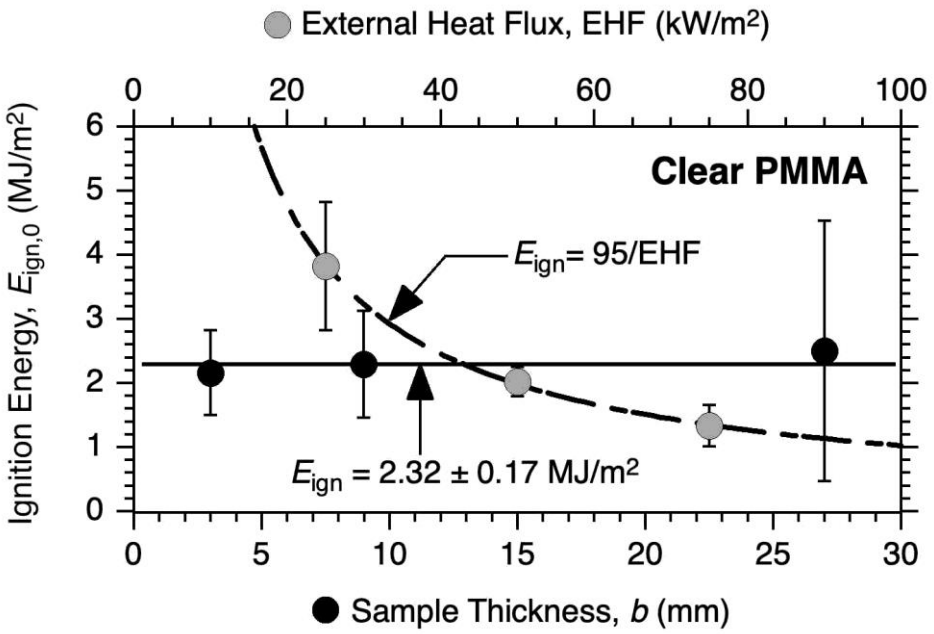

Figure 7. Apparent ignition energy $E_{ign,0}$ versus $\dot{q}_{ext}$= EHF and sample thickness (b) for clear PMMA.

Figure 8 plots $E_{ign,0,}$ and λ versus sample thickness b = 3, 9, and 27 mm and $\dot{q}_{ext}$ = 25, 50, and 75 kW/m^2 for high-impact polystyrene (HIPS) and high-density polyethylene (HDPE) in ASTM E1354 (2023). Cone data are from Stoliarov et al. (2009). Graphs for HIPS are on the left-hand side and graphs for HDPE are on the right-hand side. The $E_{ign,0}$ and λ are expected to be independent of sample thickness b according to Equations 9 and Equations 10 for thermally thick burning because δ << b and the chemical reactions that produce volatile fuel are confined to the thin surface layer (pyrolysis zone). This is indicated in Figure 8 as the horizontal line at the global mean for these non-charring polymers. The expected inverse dependence of $E_{ign,0}$ on $\dot{q}_{ext}$ as per Equation 9 is approximated for both polymers. Error bars on the data points are one standard deviation of the indicated mean with respect to the independent variable on the opposite abscissa. The EHF and b lines for $E_{ign,0}$ and λ in Figures 6-8 intersect at $\dot{q}_{ext}$ ≈ 40-50 kW/m^2 for PMMA, HIPS and HDPE.

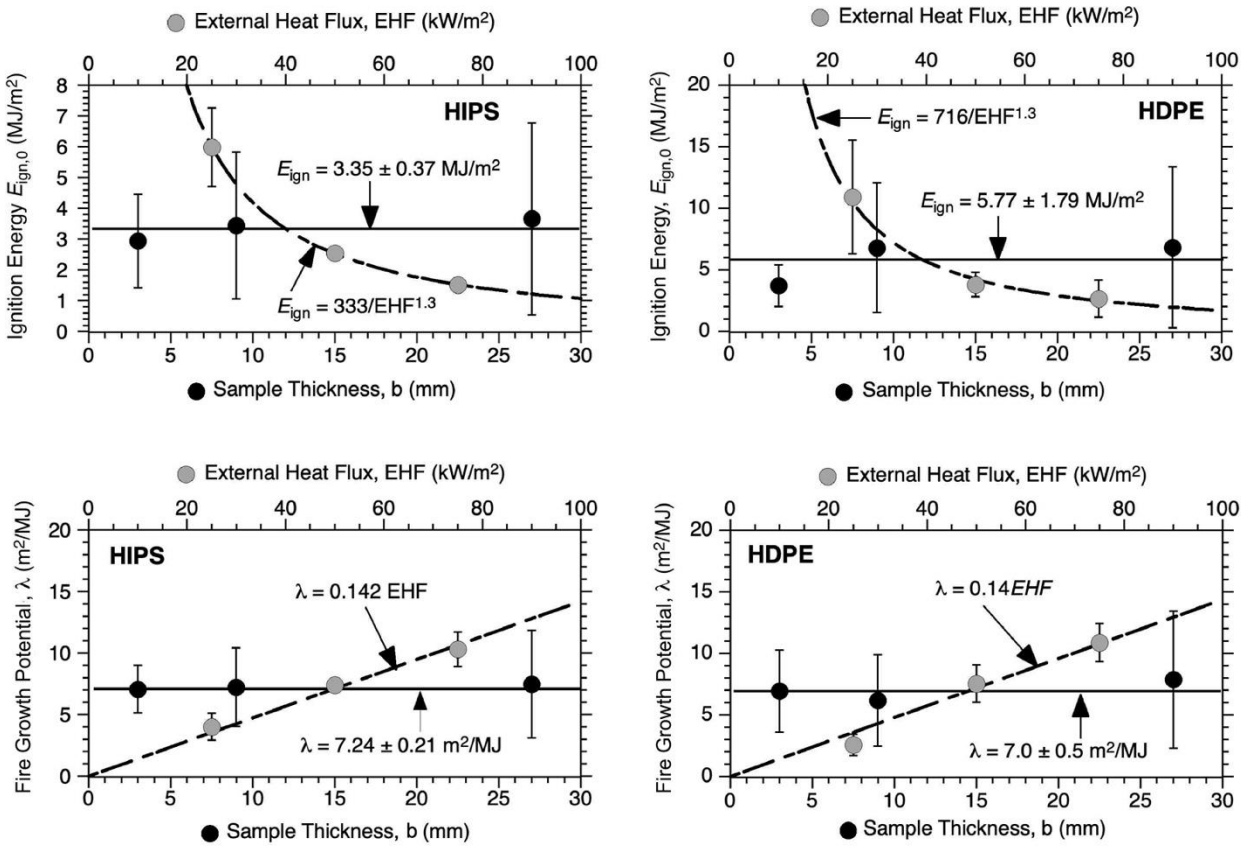

Figure 8. Apparent ignition energy $E_{ign,0}$ and fire growth potential λ of HIPS and HDPE versus $\dot{q}_{ext}$ = EHF and sample thickness (b)

5.3 Charring polymers

Combustible materials that leave a solid residue as a pyrolysis product on a burning surface do not generally exhibit steady burning due to the change in the surface boundary condition resulting from the accumulation of solid residue, which is usually of low density and insulates the underlying polymer, as well as re-radiating some of the incident energy from a heater, surface flame, or fire (Stoliarov & Ding, 2023; Stoliarov, Crowley, Walters, & Lyon, 2010) . However, the time dependent burning rate of charring materials is amenable to a moment-area representation of (steady) burning (Lyon, Crowley, & Walters, 2008) as per Equation 4. Figure 9 is a composite of heat-release rate histories for 3 mm thick samples of polycarbonate at the indicated EHF. Polycarbonate residual mass (char) fraction is μ = 0.24 (24%). Figure 10 is the energy diagram for the data in Figure 9 obtained by time integration of the ordinate $\dot{Q}$ and the abscissa $\dot{E} = \dot{q}_{ext}$. The fire growth potential of polycarbonate $\lambda_{NRG} = (\Delta Q/\Delta E_0)/E_{ign,0}$ is plotted in Figure 11 along with λ_{max} for polycarbonate from three laboratories (Hirschler, 1992; Lyon & Crowley, 2021; Bundy & Ohlemiller, 2003; ASTM E1354, 2023) . There is good overall agreement between λ for the individual laboratories, with low sensitivity of λ to $\dot{q}_{ext}$ due to the

insulating and reradiating effect of the intumescent surface char. The nominal ignition energy $E_{ign,0}$ at each b and $\dot{q}_{ext}$ for polycarbonate of Bisphenol-A (PC) in ASTM E1354 (2023) are plotted in Figure 12 (Hirschler, 1992; Lyon & Crowley, 2021; Stoliarov, Crowley, Walters, & Lyon, 2010) showing a similar weak dependence of EHF and b on $E_{ign,0}$ and an intersect of these lines at $\dot{q}_{ext}$ = 70 kW/m^2.

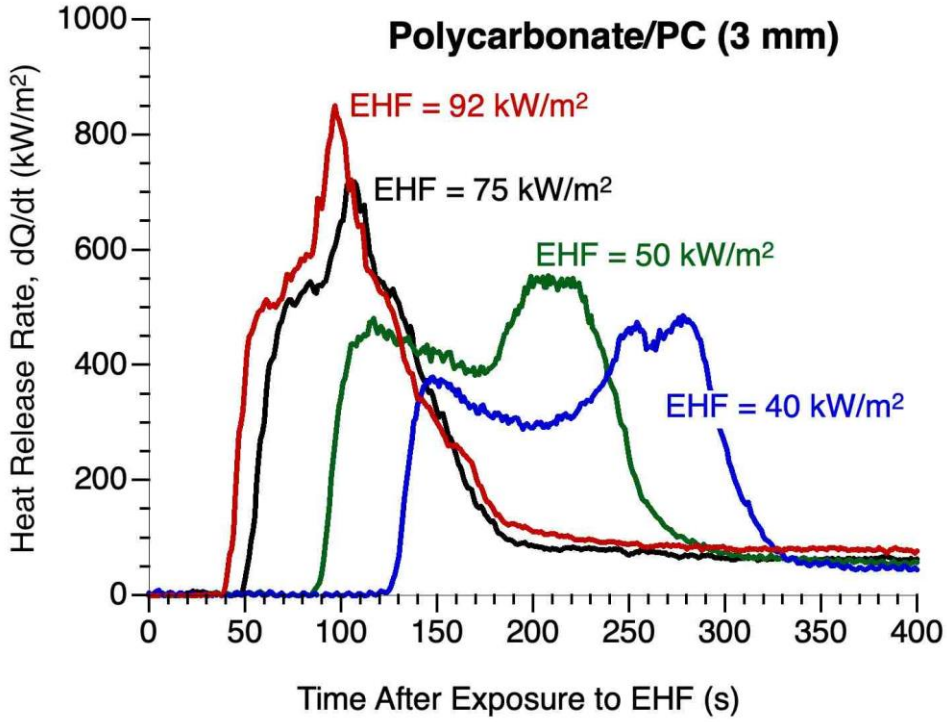

Figure 9. Heat release rate histories of 3 mm polycarbonate at indicated $\dot{q}_{ext}$= EHF.

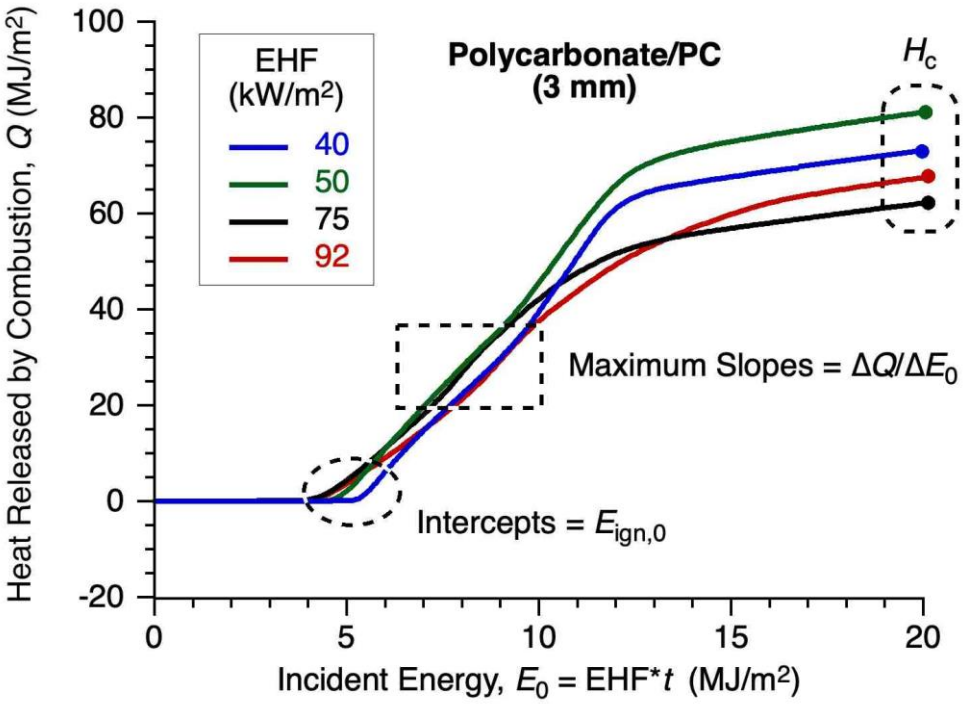

Figure 10. Cone calorimeter energy diagram of heat release Q versus incident energy E_0 showing nominal ignition energy $E_{\text{ign},0} = \dot{q}_{ext} t_{ign}$ and combustibility, $\Delta Q/\Delta E_0$.

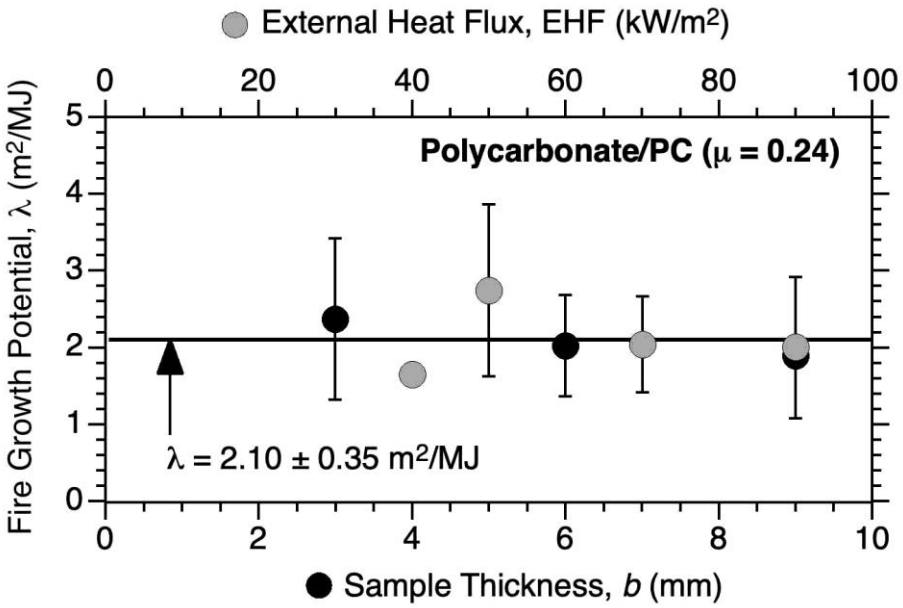

Figure 11. Fire growth potential λ versus $\dot{q}_{ext}$= EHF and sample thickness (b) for PC from three different laboratories

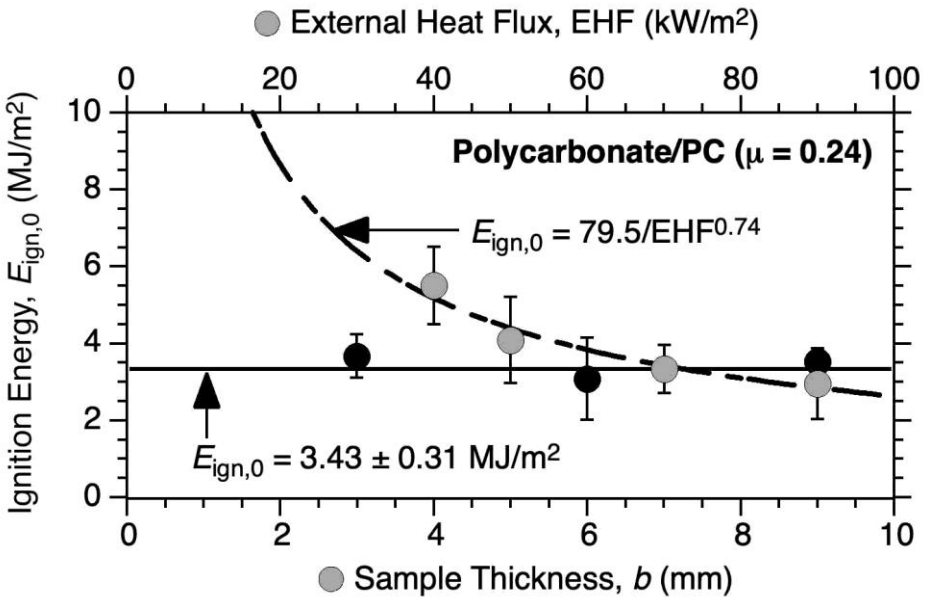

Figure 12. Apparent ignition energy $E_{ign,0}$ versus $\dot{q}_{ext}$ = EHF and sample thickness (b) for PC

The graphs on the left-hand side of Figure 13 (ASTM E1354, 2023) are plots of $E_{ign,0}$ and λ versus b and $\dot{q}_{ext}$ for rigid, unplasticized polyvinylchloride (PVC). The lower char yield (μ = 0.19) and smaller volumetric expansion of PVC compared to PC (μ = 0.24) shows the expected independence of λ from b and linear dependence of λ on $\dot{q}_{ext}$ as per Equation 10, while $E_{ign,0}$ is inversely related to $\dot{q}_{ext}$ as per Equation 9. At the crossover points, $\dot{q}_{ext}$ = 78-80 kW/m^2.

The graphs on the right-hand side of Figure 13 are plots of $E_{ign,0}$ and λ versus b and $\dot{q}_{ext}$= EHF for polyetheretherketone (PEEK). The high char yield (μ = 0.50) and voluminous char swelling of PEEK obscures any dependence of $E_{ign,0}$ and λ on b and $\dot{q}_{ext}$, so the horizontal dashed lines are global averages of $E_{ign,0}$ and λ. Error bars on the data points are one standard deviation of the mean with respect to the independent variable on the opposite abscissa.

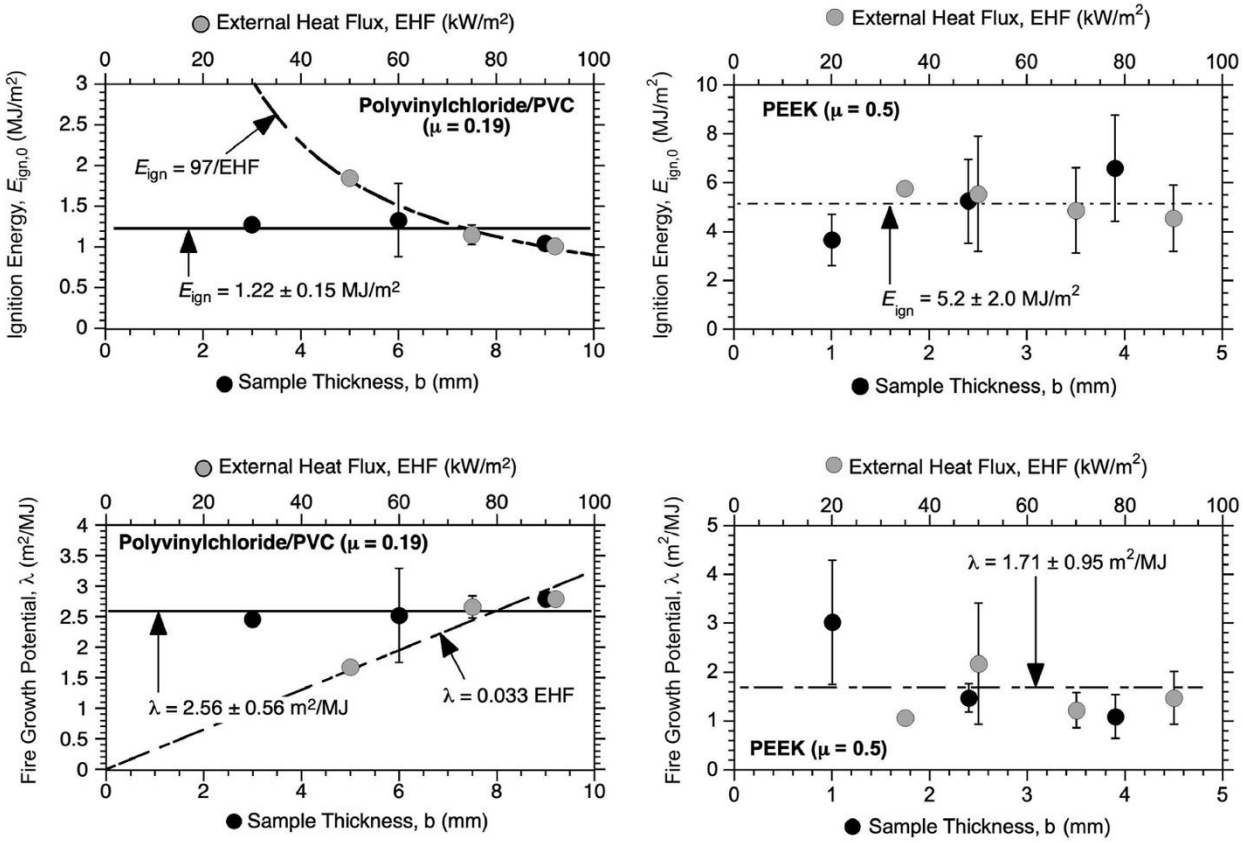

Figure 13. Nominal ignition energy $E_{ign,0}$ and fire growth potential λ of PVC and PEEK versus $\dot{q}_{ext}$= EHF and sample thickness (b) in ASTM E1354

5.4 Applications

Figure 14 is a plot of λ and Π for blends of acrylonitrile-butadiene-styrene polymer (ABS) with polycarbonate (PC) tested in our laboratory in triplicate as 3.2 mm thick samples at $\dot{q}_{ext}$ = 50 kW/m^2 in the cone calorimeter. Both λ and Π of the blends increase monotonically according to a lower bound rule of mixtures as the weight fraction of the non-charring, more easily ignited, and highly combustible ABS increases (see Figure 4 and Figure 15).

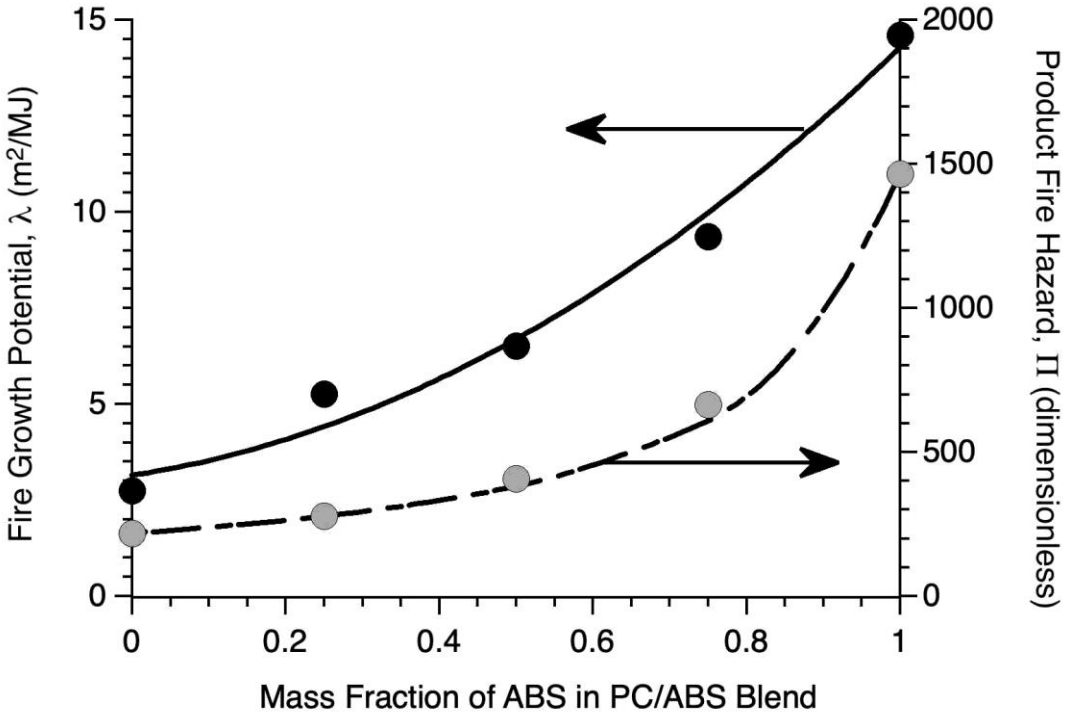

Figure 14. Fire growth potential (λ) and product fire hazard (Π) of PC/ABS blends

Figure 15 is a plot of the material fire hazard of various samples computed from cone calorimeter data in the literature (Hirschler, 1992; Lyon, et al., 1997), as $\pi = \lambda H_c/b = \Pi/b$, from Equation 13. The data from Hirschler is an average value of π measured at $\dot{q}_{ext}$= 40 kW/m^2 and 70 kW/m^2, while π for the composites from Lyon et.al are average values for the nominal resin system at an external heat flux, $\dot{q}_{ext}$ = 50 kW/m^2. These π values are intensive properties that span 4 decades in Figure 15. The π property is intensive because it is independent of the amount (thickness) of material.

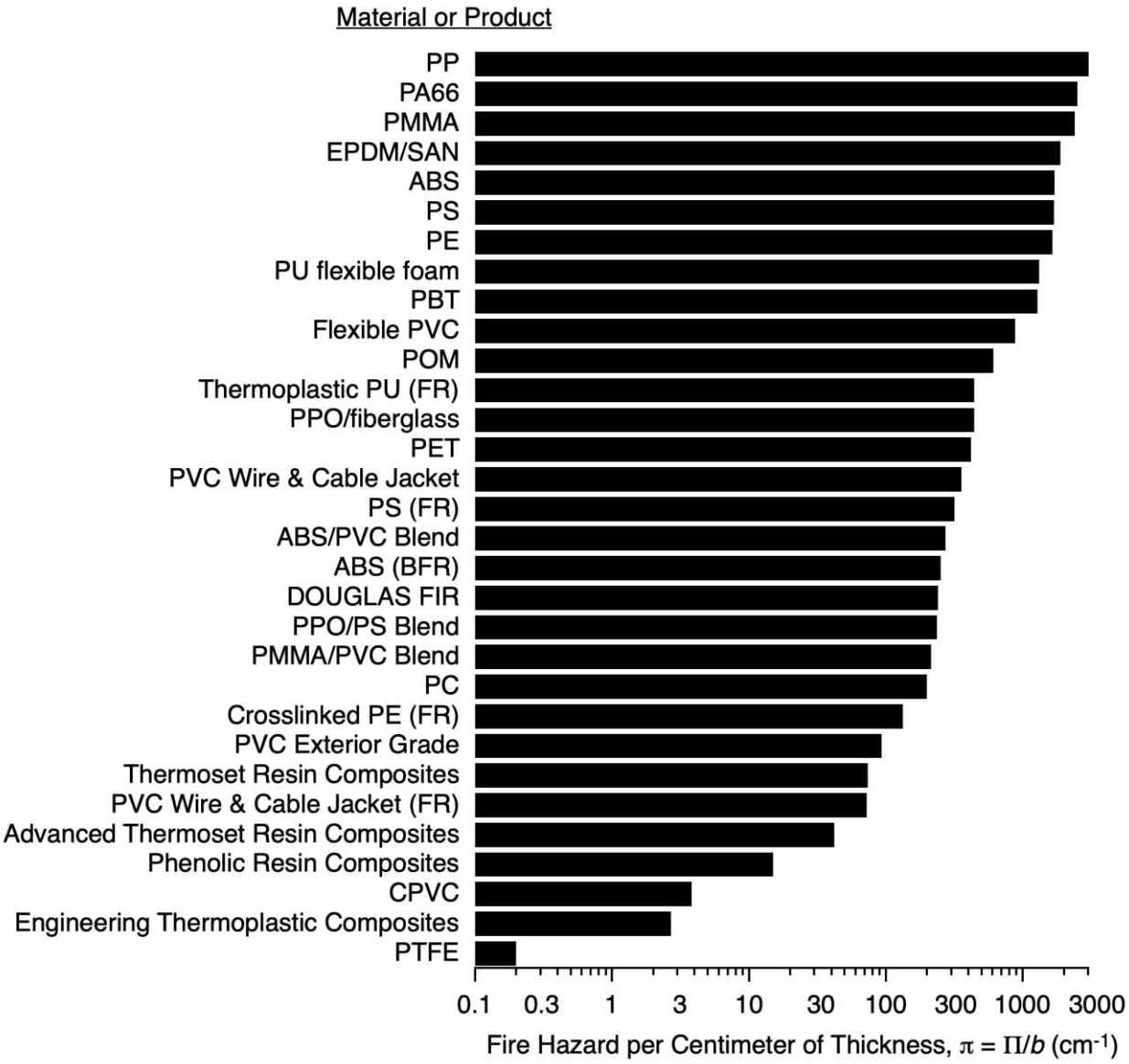

Figure 15. Material fire hazard, $\pi = \Pi/b$ (cm^{-1})

Figure 16 is a plot of the material fire hazard, $\pi = \Pi/b$ (MJ/m^3) of pure polymers and polymer blends measured in a bench-scale (cone) calorimeter versus the specific fire growth capacity, FGC (J/g-K) (Lyon, Safronava, Crowley, & Walters, 2021), measured in a micro (10^{-6} kg) scale combustion calorimeter according to ASTM D7309 (2023).The line through data points is a power law fit having correlation coefficient R = 0.82. Figure 16 shows qualitative correlation between the intensive bench scale fire property π and the intensive microscale/molecular property FGC, which reinforces the hypothesis that the volumetric fire hazard π is a material

parameter that can be measured in a cone calorimeter and used for comparison, classification, and ranking of the level of passive fire protection afforded by materials and products.

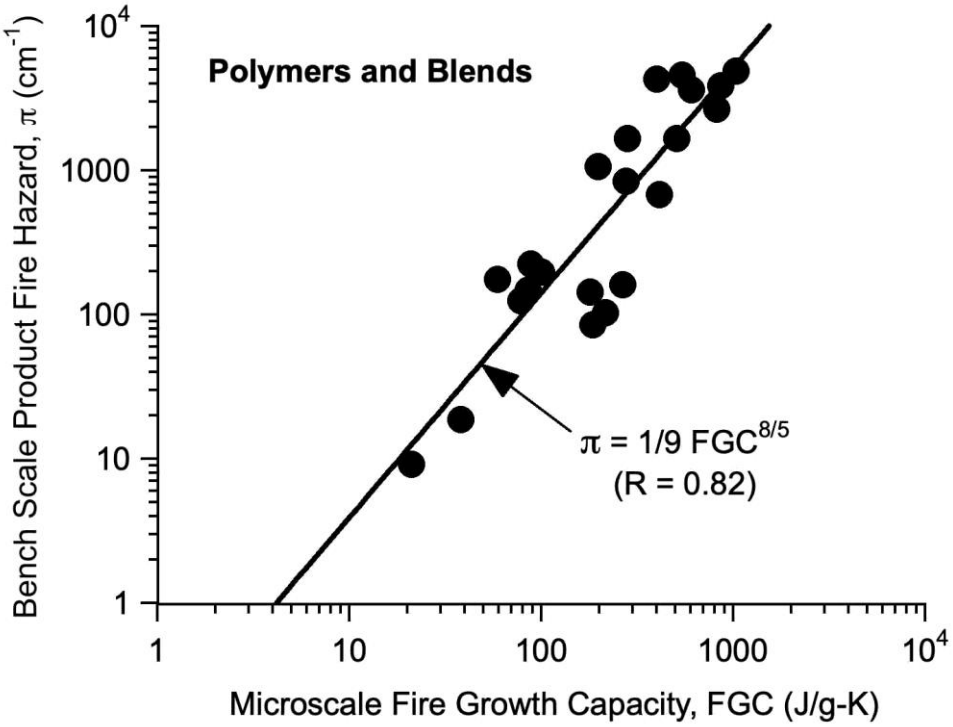

Figure 16. Bench scale product fire hazard π (cm^{-1}) versus microscale fire growth capacity FGC (J/g-K) for 22 polymers and polymer blends.

Figure 17 is a graphical summary of the data obtained by Hong et.al. (2004) in a study of the effectiveness of phosphorus and bromine-containing flame-retardant additives on the fire growth of free-standing, isolated computer monitors, and television sets subjected to three small, open flame ignition sources for 1.5 to 5 minutes, or until ignition occurred. The 2.1 mm thick housings for the monitor and TV were commercial materials containing either no flame retardant (NFR), a phosphorus flame retardant (PFR), or a brominated flame retardant (BFR). The housings were tested separately as rectangular bars in the UL 94 flammability test (2023) of upward flame spread, the limiting oxygen index (LOI) test of downward flame spread (ASTM D2863-23, 2023), and as 10 cm square plates in a cone calorimeter at $\dot{q}_{ext}$ = 50 kW/m^2 according to the standard method (ASTM E1354, 2023). The full-scale test results are plotted in Figure 17 as reported: either no sustained burning (B = 0) or as a fully developed product fire (B = 1). These results were fit to a conditional probability function (Lyon & Safronava, 2013) with Π as the sole explanatory variable,

$$P = p(B|\Pi) = \frac{1}{1+(\Pi^*/\Pi)^m} \quad (22)$$

Equation 22 is the likelihood, *P*, which sustained burning, B, will occur in a full-scale fire test of a product having fire hazard, Π. The binary full-scale results were fit to Equation 22, and the solid line in Figure 17 (Hong, Yang, Ahn, Mun, & Lee, 2004) is the result for non-linear regression values, Π* = 765 and *m* = 27. Figure 17 indicates that computer monitors and televisions with housings containing phosphorus flame retardants exhibit a loss of passive fire protection (*P* = ½) at Π = 765 or $\lambda \approx 8$ m^2/MJ, as evidenced by a transition from no sustained burning (no fire growth) to sustained burning culminating in a fully developed fire. The UL 94 vertical flammability classifications and flame-retardant additive for the housings are indicated in Figure 17. No sustained burning is observed for V-0, V-1 classifications containing PFR or BFR additives. Fully developed fires are observed for V-2 and HB classifications containing PFR or NFR additives. These UL 94 V classifications of passive fire protection are consistent with the IEC 62368-1 (2023) fire safety requirement for computer and television housings.

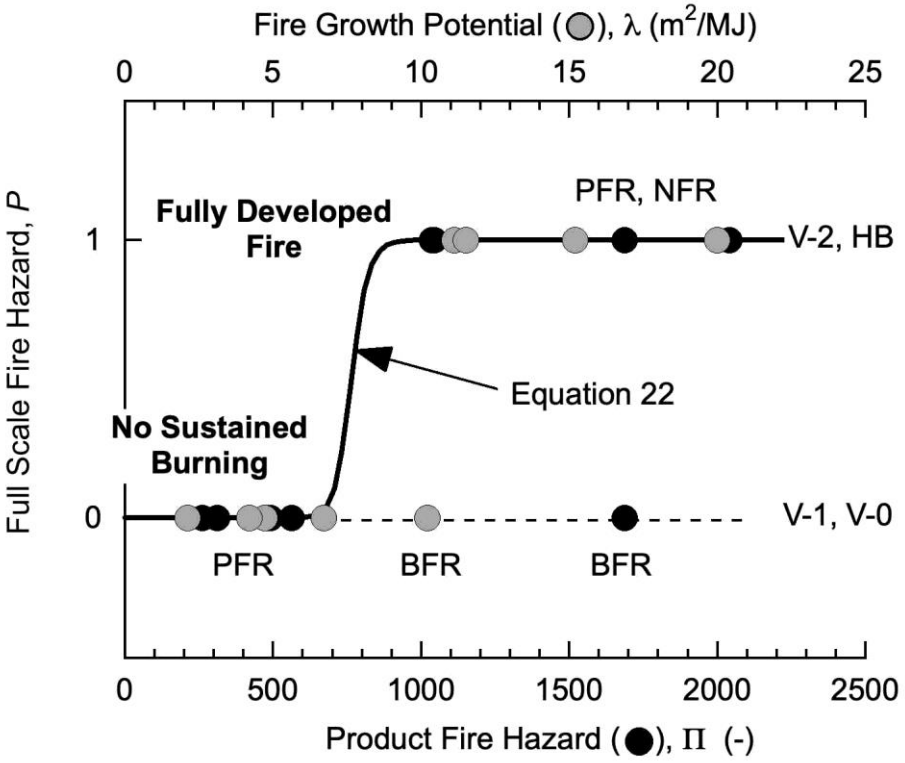

Figure 17. Results of product fire testing of computer monitors and televisions having polystyrene housings containing NFR, PFR, or BFR

Figure 18 is a graphical summary of the data from a study performed at the National Institute of Standards and Technology (NIST) on the effect of flame-retardant housings of computer monitors on the full-scale fire hazard of these products (Bundy & Ohlemiller, 2004). The 3.2 mm thick computer housings were tested separately in a cone calorimeter at $\dot{q}_{ext}$ = 50 kW/m^2 by the standard method (ASTM E1354, 2023), as well as in the UL 94 (2023) vertical test of plastic flammability. The products were tested as isolated, free-standing units under a large hood so that heat release rate could be measured by oxygen consumption. Products were subjected to a small open flame for 0.3 to 7 minutes until ignition occurred. The results were reported as no sustained fire growth after ignition (B = 0) or a fully developed fire (B = 1) having a heat release rate greater than 200 kW. The solid line in Figure 18 is a fit of Equation 22 to the binary full-scale data using non-linear regression values, Π* = 754 and m = 46. The results in Figure 18 are consistent with Figure 17 in that there is no fire propagation of the isolated, free-standing monitors for UL 94 V-1, V-0, while fire growth to a fully developed fire is observed for UL 94 V-2 and HB, regardless of the type of fire-retardant additive.

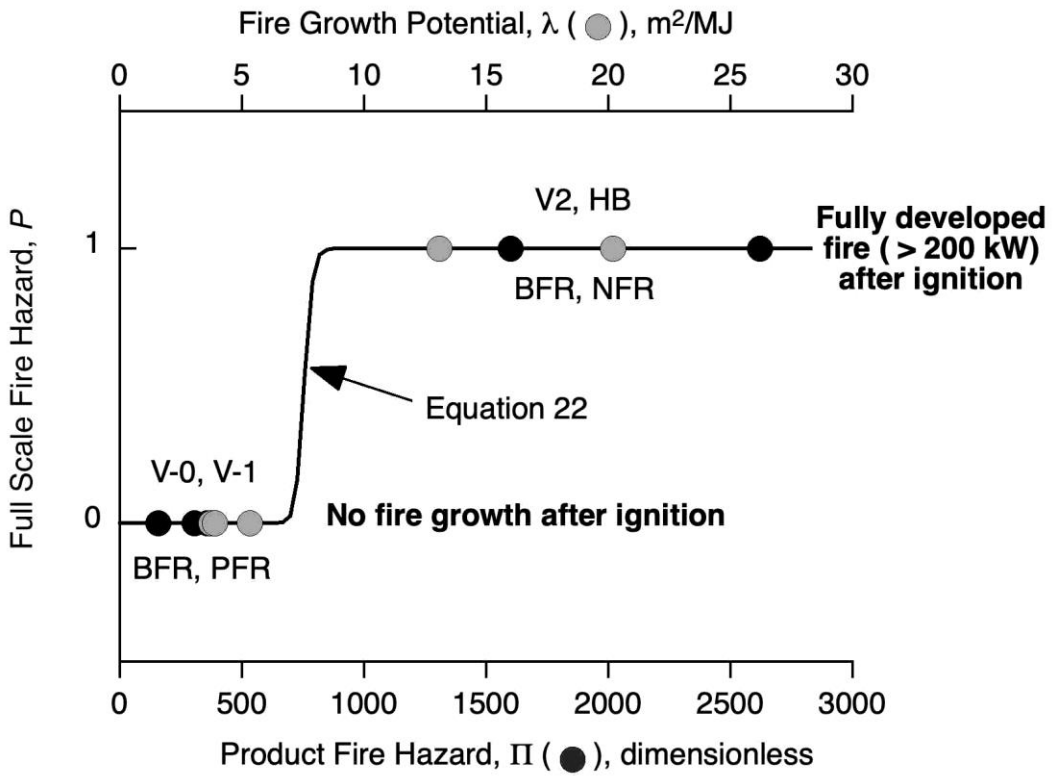

Figure 18. Results of product fire testing of computer monitors having plastic housings containing NFR, PFR, or a BFR

Figure 19 is a summary of the UL 94 vertical classification reported in Hong, et al. (2004) and Bundy& Ohlemiller (2003) versus the fire growth potential λ and product fire hazard Π computed using Equations 20 and 21 , respectively, from the cone calorimeter data reported for 1.6, 2.1, and 3.2-mm thick samples of PC, HIPS, ABS, PC/ABS, PP, and PS tested as natural materials with no flame retardants (NFR) or modified with non-halogen (mainly phosphorus) (PFR) and bromine-containing flame retarding (BFR) additives. The poor correlation of λ and Π with UL 94V classifications in Figure 19 is inconsistent with the success of UL94V as a predictor of full-scale fire growth as a categorical outcome in Figure 17 and Figure 18. The reason for these differences is the pronounced effect of sample thickness, loss of physical integrity of melting samples, and three-dimensional burning on the UL 94V classification- none of which influence λ and Π in forced, one-dimensional, horizontal burning in the cone calorimeter.

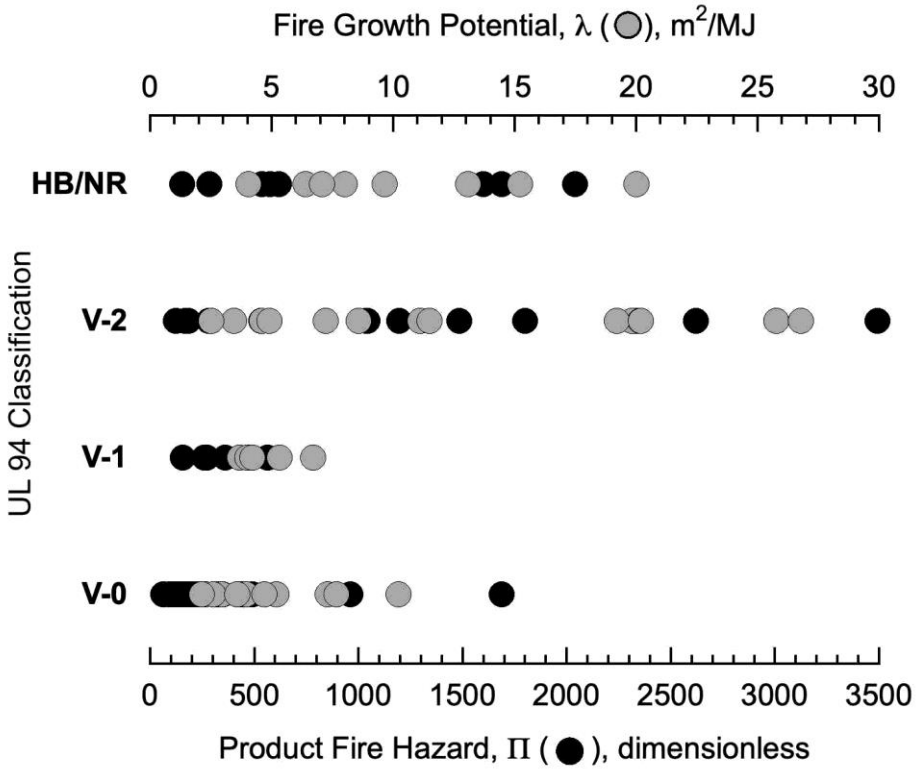

Figure 19. UL 94V classification versus fire growth potential (λ) and product fire hazard (Π).

Figure 20 is a plot of measured (black circles) and estimated (gray circles) times to flashover for natural and flame-retardant wood products in the ISO 9705 (2016) room corner fire test versus the product fire hazard Π computed from the published cone calorimeter data for these products

(Ostman & Tsantaridis, 1994; 1995)Time to flashover in this test is defined as the time to reach a heat release rate of 1-MW in a standard 2.4-m wide x 2.4-m high x 3.6-m deep room lined with test materials on both walls and the ceiling of a corner that is ignited at the bottom with a propane burner in 10-minute sequences of 100 and 300 kW. The test is used to classify building products in Europe for early-stage fire growth potential The empirical relationship used to estimate the times to flashover for wood and other products that were not tested (gray circles) was, $t_{FO}(s) = (0.07 t_{ign}^{0.25} \rho^{1.7}/THR^{1.3}) + 60s$ (Ostman & Tsantaridis, 1994), based on a correlation of the time to flashover in the ISO 9705 (2016) room fire test for 28 materials having density ρ and for which the time-to-ignition t_{ign} and total heat release THR at 300 seconds were measured in a cone calorimeter at $\dot{q}_{ext}$ = 50 kW/m^2 according to the standard method (ISO-5660-1, 2002). The trend of the measured and estimated t_{FO} versus Π shown in Figure 20 indicates that the rate of decrease in the time to flashover at 1 MW in the ISO 9705 room corner fire test is inversely proportional to Π, i.e.,

$$-\frac{dt_{FO}}{d\Pi} \propto \frac{1}{\Pi} \equiv \frac{t_0}{\Pi} \tag{23}$$

Separating variables in Equation 23 and integrating from an initial condition, Π_0 at t_0,

$$t_{FO} = t_0 \left(1 + \ln\left[\frac{\Pi_0}{\Pi}\right]\right) \tag{24}$$

The solid line through the data points in Figure 20 is Equation 24 with nonlinear regression parameters, $\Pi_0 = 200$ at $t_0 = 2$ minutes. The correlation coefficient of Equation 24 to the measured t_{FO} with these parameters is R = 0.90. Products with $t_{FO} \geq 10$ minutes receive the highest safety rating (Class 1) in the British, French, German, and Scandinavian fire standards, corresponding to $\Pi \leq 75$ as the sole explanatory variable.

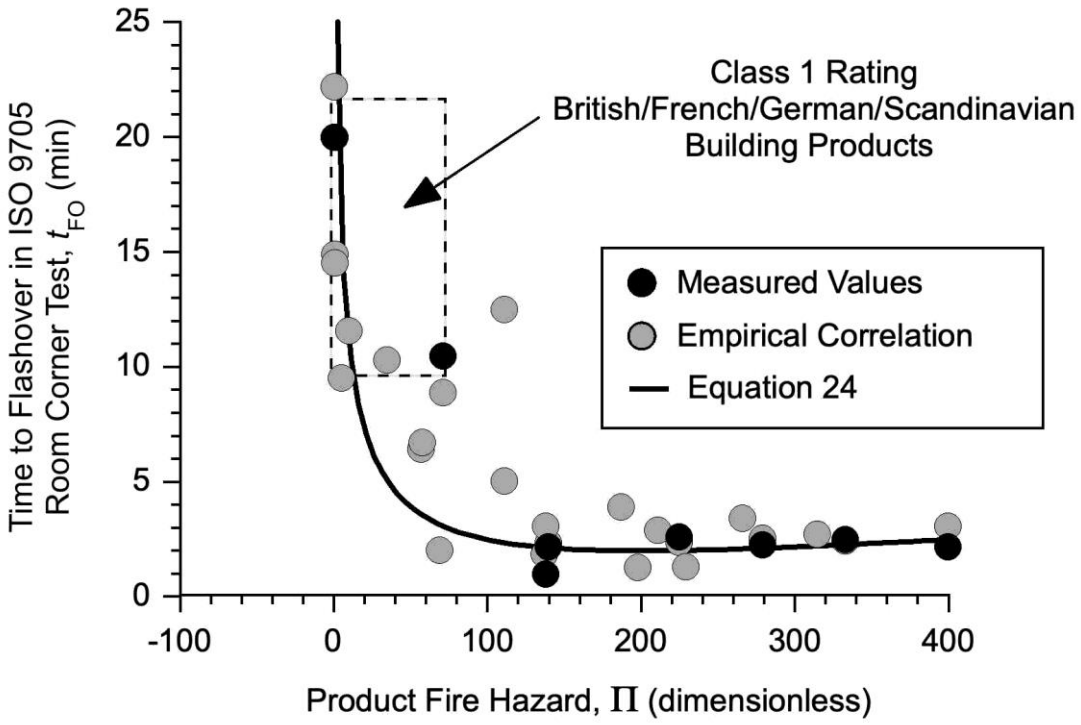

Figure 20. Time to flashover t_{FO} in the ISO 9705 room fire test versus product fire hazard Π for building products.

Figure 21 is a plot of the fraction of the metrics in regulatory bench-scale fire tests (Marker, 2019) that combustible materials must pass (expressed as a percentage) versus Π for the material in a cone calorimeter at an external energy flux, $\dot{q}_{ext}$ = 50 kW/m^2. The regulatory bench-scale fire test metrics included in the study that were compared to acceptable values include the results of the vertical flammability test with a 12s Bunsen burner ignition, the peak rate of heat release in 5-minutes and the total heat released at 2-min in the Ohio State University fire calorimeter, the burn length and after-flame time in the radiant panel horizontal flame spread test, as well as the amount of smoke generated in forced flaming combustion at an external energy flux, $\dot{q}_{ext}$= 25 kW/m^2. The efficacy of the product fire hazard Π as the sole indicator of passive fire protection is demonstrated by the highly correlated (R^2 = 0.93) trend line through the data points in Figure 21. Likelihood (expressed as a percentage) that a combustible product having fire hazard Π will pass all of the FAR flammability requirements for aircraft cabin materials. The trend line is the solution to $-dN/d\Pi = N/\Pi_0$, where N is the percentage of passing FAR flammability tests for a product having fire hazard Π and Π_0 is a characteristic value for the data set. By this method of accounting, N/N_0 is essentially the likelihood that a combustible material having fire growth

potential Π will pass all the bench-scale flammability metrics for a material used in aircraft cabin interiors.

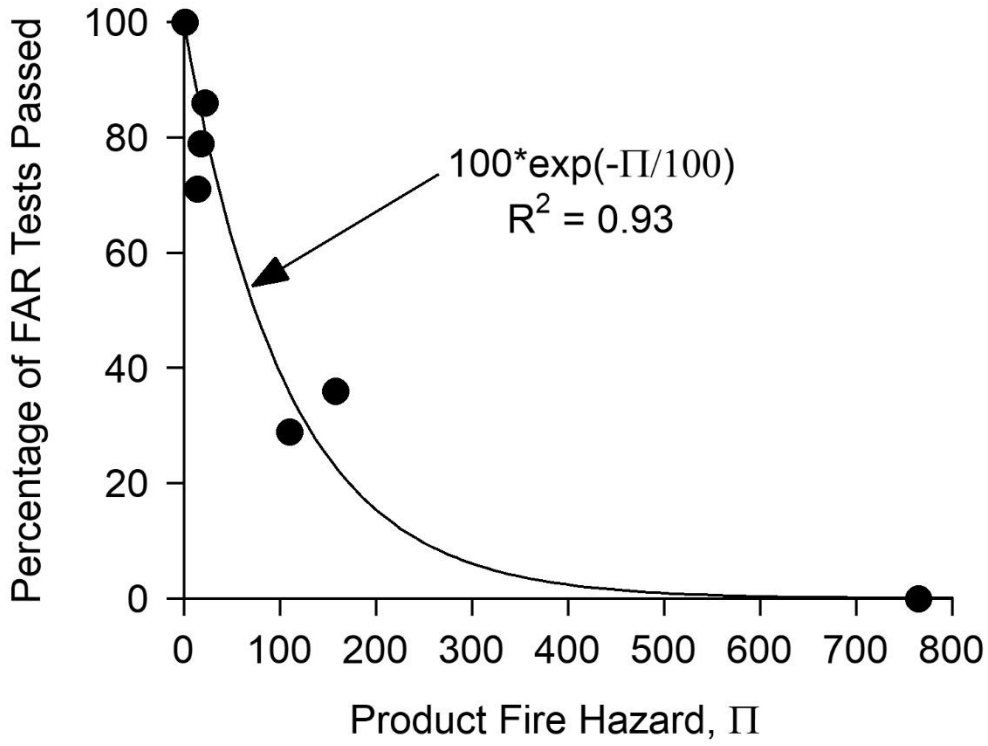

Figure 21. Likelihood (expressed as a percentage) that a combustible product having fire hazard Π will pass all of the FAR flammability requirements for aircraft cabin materials.

6 Summary and conclusions

The coupled fire growth processes of surface flame-spread and in-depth burning of combustible solids are accounted for in the fire growth potential λ (m^2/MJ) which is the increase in surface flame spread rate (m^2/s) per unit increase in the radiant power of a fire or heater (W). In integral form λ is the product of ignitability and burning rate computed from the heat release rate history in a cone calorimeter at an external energy flux $\dot{q}_{ext}$ that is above the critical energy flux for ignition and burning, $\dot{q}_{burn}$

$$\lambda \equiv \ Ignitability * Burning\ Rate = \left(\frac{1}{E_{ign}}\right)\left(\frac{\Delta Q}{\Delta E_0}\right) \approx \left(\frac{1}{\dot{q}_{ext} t_{ign}}\right)\left(\frac{\dot{Q}_{max}}{\dot{q}_{ext}}\right)$$

The ignition energy, $E_{ign} = \dot{q}_{ext} t_{ign}$ (MJ/m^2) is the barrier to the initiation of surface flame spread while the burning rate that drives flame spread is proportional to the dimensionless combustibility, $\Delta Q/\Delta E_0 \approx H_c/H_g$. The product of these terms is a constitutive relationship for the

fire response of a combustible solid to the thermal stress of a fire or heater $\dot{q}_{ext}$ in the coupled fire growth process, because the fire compliance *K* is an intensive material property,

$$\lambda = \left[\frac{h_c/h_g}{\kappa\rho c_P \Delta T_{ign}^2}\right]\dot{q}_{net} = K\left(\dot{q}_{ext} - \dot{q}_{ign}\right)$$

The experimental data in Figures 6-8 indicate that an external energy flux, $\dot{q}_{ext} \approx 45 \pm 5$ kW/m^2, is necessary for sustained burning of non-charring polymers in the cone calorimeter, while Figures 12 and 13 indicate $\dot{q}_{ext} = 75 \pm 5$ kW/m^2 is necessary for sustained burning of charring polymers. The observation that the energy flux for burning is higher than that for ignition follows directly from the fire growth constitutive relationship, Equation 10,

$$\dot{q}_{ext}(burning) \equiv \dot{q}_{burn} = \dot{q}_{ign} + \frac{\lambda}{K} \qquad 25$$

The potential of a combustible solid to grow a fire is only realized as a hazard if its heat of combustion is sufficient to sustain fire growth. For a product having areal heat of combustion, H_c (MJ/m^2) the dimensionless fire hazard is, $\Pi = \lambda H_c$, which is an extensive property because it depends on the amount (thickness) of the sample.

The product fire hazard Π successfully correlates the categorical outcome of fire tests of free standing telecommunication equipment (Figure 17 and 18), the fire growth rate of building and wall lining materials in a full-scale ISO 9705 room fire test (Figure 20), and the likelihood that an aircraft cabin material will pass all of the FAR flammability requirements (Figure 21) when used as the sole explanatory variable. The magnitude of Π at the onset of fire growth is scenario/test dependent. For example, $\Pi \approx 750$ is sufficient fire protection for free standing telecommunication products, while, $\Pi \approx 75$, is necessary for building materials and wall linings to withstand the more severe thermal insult of a compartment fire (room or aircraft cabin).

The material fire hazard, $\pi = \Pi/b$, is an intrinsic measure of flammability as evidenced by its ranking of the observed performance of polymers in small- and bench-scale flammability tests (Figure 15) as well as its correlation with the molecular-level FGC of polymers (Figure 16).The material fire hazard π is an intensive property that is useful for ranking material fire performance (Figure 15) because it is independent of the amount of sample.

7 References

Agarwal, G., Wang, Y., & Dorofeev, S. (2021). Fire performanace evaluation of cladding wall assemblies using the 16-ft high parallel panel test method of ANSI/FM 4880. *Fire and Materials, 45*, 609-623.

ANSI/FM Approvals 4910-2004. (2004). *American national standard for clean room materials flammability test protocol.* Norwood, MA: FM Approvals LLC.

ASTM 2257. (2022). *Standard test method for room fire test of wall and ceiling materials and assemblies.* West Conshohocken, PA: ASTM International.

ASTM D2863-23. (2023). *Standard test method for measuring the minium oxygen concentration to support candle-like combustion of plastics (Oxygen index).* West Conshohocken, PA: ASTM International.

ASTM D7309-23. (2023). *Standard test method for determining flammability characteristics of plastics and other solid materials using microscale combustion calorimetry.* West Conshohocken: ASTM International .

ASTM E1354. (2023). *Standard test method for heat and visible smoke release rates for materials and productions using an oxygen consumption calorimeter.* West Conshohocken, PA: ASTM International.

ASTM E2058. (2019). *Standard test methods for measurement of material flammability using a fire propagation apparatus (FPA).* West Conshohocken, PA: ASTM International.

ASTM E906. (2017). *Standard test method for heat and visible smoke release for materials and products using a thermopile method.* West Conshohocken, PA: ASTM International.

Bundy, M., & Ohlemiller, T. (2003). *Bench scale flammability measures of electronic equipment.* Gaithersburg, MD: National Institute of Standards and Technology Interagency/Internal Report, NISTR 7031.

Bundy, M., & Ohlemiller, T. (2004). *Full-scale flammability measures for electronic equipment, Technical note TN 1461.* Gaithersburg, MD: National Institute of Standards and Technology.

CEN-EN 13823:2020+A1:2022. (n.d.). *Reaction to fire tests for building products - excluding floorings - exposed to the thermal attack by a single burning item.*

Compartment Interiors, 14 CFR 25.853 (2004).

Drysdale, D. D. (2011). *An introduction to fire dynamics, Third edition, Chapter 5 & 6.* Sussex, UK: John WIley & Sons, Ltd.

Hirschler, M. M. (1992). Heat release from plastic materials. In *Heat Release from Fires.* Essex, England: Elsevier Applied Science, V Babrauskas & SJ Grayson, eds.

Hirschler, M. M. (1995). Analysis of heat release and other data from a series of plastic materials tested in the cone calorimeter. *20th INternational Conference on Fire Safety, January 9-13.* San Francisco, CA.

Hong, S., Yang, J., Ahn, S., Mun, Y., & Lee, G. (2004). Flame retardancy performance of various UL94 classified materials exposed to external ignition sources. *Fire and Materials, 21*, 25-31.

IEC62368-1. (2023). *Safety requirements for audio/video, Information and communications technology.* International Electrotechnical Commission.

ISO 9705-1. (2016). *Full scale room test for surface products.* Geneva, Switzerland: International Organization for Standardization.

ISO-5660-1. (2002). *Reaction-to-fire tests-heat release, smoke production and mass loss rate :Part 1(cone calorimeter method)* . Geneva, Switzerland: International Organization for Standardization.

Lyon, R. E. (2000). Heat release kinetics. *Fire and Materials, 24*, 179-186.

Lyon, R. E., & Crowley, S. (2021). Fire properties of combustible materials from unsteady burning. *Fire Safety Journal, 120,* 103054.

Lyon, R. E., & Safronava, N. (2013). *A probabilistic analysis of pass/fail fire tests, Final report (DOT/FAA/TC-12/13]*. Federal Aviation Administration .

Lyon, R. E., Balaguru, P. N., Foden, A., Sorathia, U., Davidovits, J., & Davidovits, M. (1997). Fire resistant aluminosilicate composites. *Fire and Materials, 21*, 67-73.

Lyon, R. E., Crowley, S., & Walters, R. (2008). Steady heat release rate by the moment area method. *Fire and Materials, 32,* 199-212.

Lyon, R. E., Safronava, N., & Crowley, S. (2018). Thermal analysis of polymer ignition. *Fire and Materials, 42*, 668-679.

Lyon, R. E., Safronava, N., Crowley, S., & Walters, R. N. (2021). A molecular-level fire growth parameter. *Polymer Degradation and Stability, 186,* 109478.

Marker, T. R. (2019). *Aircraft materials fire test handbook, Revision 3 [DOT/FAA/TC-17/55]*. Federal Aviation Administration.

McGrattan, K., McDermott, R., Weinschenk, C., & Forney, G. (2013). *Fire dynamics simulator users guide, sixth edition, special publication (NIST SP 1019).* Gaithersburg, MD: National Institute of Standards and Technology.

NFPA 286. (n.d.). *Corner room fire test for interior wall and ceiling.* IBC Chapter 8 Section 803.

Nguyen, H. T., Nguyen, K., Le, T. C., & Zhang, G. (2021). Review on the use of artificial intelligence to predict fire performance of construction materials and their flame retardancy. *Molecules, 26*(4), 1022.

Numjiri, F., & Furukawa, K. (1998). Short communication: Mathematical expression of heat release rate curve and proposal of "Burning index". *Fire and Materials, 22*, 39-42.

Ostman, B., & Tsantaridis, L. D. (1994). Correlation between cone calorimater data and time to flashover in the room fire test. *Fire and Materials, 18*, 205-209.

Ostman, B., & Tsantaridis, L. D. (1995). Heat release and classification of fire retardant wood products. *Fire and Materials, 19*, 253-258.

Petralla, R. V. (1994). The assessment of full-scale fire hazards from cone calorimeter data. *Journal of Fire Sciences, 12*, 14-43.

Quintiere, J. G. (2006). *Fundamentals of Fire Phenomena, Chapter 7 & 9.* Sussex, UK: John Wiley & Sons, Ltd.

Rasbash, D. J. (1976). Theory in the evaluation of fire properties of combustible materials. *Proceedings 5th International Fire Protection Seminar*, (pp. 113-130). Karlsruhe, Germany.

Shields, T. J., Silcock, G. W., & Murray, J. J. (1994). Evaluating ignition data using the flux time product. *Fire and Materials, 18*, 243-254.

Stoliarov, S. I., & Ding, Y. (2023). Pyrolysis model parameterization and fire growth predictiona: The state of the art. *Fire Safety Journal, 140*, 103905.

Stoliarov, S. I., Crowley , S., Lyon, R. E., & Linteris, G. T. (2009). Prediction of burning rates of non-charring polymers. *Combustion and Flame, 156*, 1068-1083.

Stoliarov, S. I., Crowley, S., Walters, R. N., & Lyon, R. E. (2010). Prediction of the burning rates of charring polymers. *Combustion and Flame, 157*, 2024-2034.

Stoliarov, S. I., Leventon, I. T., & Lyon, R. E. (2013). Two-dimensional model of burning for pyrolyzable solids. *Fire and Materials, 38*(3), 391-408.

Tewarson, A. (1980). Heat release rate in fires. *Fire and Materials, 4*(4), 185-191.

Tewarson, A. (1994). Flammability paramters of materials: Ignition, combustion, and fire propagation. *Journal of Fire Sciences, 12*, 329-356.

Tewarson, A., Kahn, M., Wu, P. K., & Bill, Jr., R. G. (2001). Flammability evaluation of clean room products for the semiconductor industry. *Fire and Materials, 25*, 31-42.

Underwriters Laboratories. (2023). *UL 94 test for flammability of plastic materials for parts in devices and appliances.* Northbrook, IL.

Vahabi, H., Kandola, B. K., & Saeb, M. R. (2023). Flame retardancey index (FRI) for polymer material ranking. *Polymers, 15*, 2422.

Vahabi, H., Movahedifar, E., Kandola, B. K., & Saeb, M. R. (2019). Flame retardancy index (FRI) for thermoplastic composites. *Polymers, 11*, 407.

Van Hees, P., Hertzberg, T., & Steen, H. A. (2002). *Development of a screening method for the SBI and room corner using the cone calorimeter (SP Report 2002:11).* Sweden: SP Fire Technology.

Whiteley, R., Elliot, P., & Staggs, J. (1996). Steady State Analysis of Cone Calorimeter Data. In *Flame Retardants* (Vol. 7, pp. 71-78).